

# Condition for dust evacuation from the first galaxies

Hajime Fukushima<sup>1</sup>\* Hidenobu Yajima<sup>2,3</sup> Kazuyuki Omukai<sup>2</sup>

<sup>1</sup>*Department of Physics, Kyoto University, Sakyo, Kyoto 6060-8502, Japan*

<sup>2</sup>*Astronomical Institute, Tohoku University, Aoba, Sendai 980-8578, Japan*

<sup>3</sup>*Frontier Research Institute for Interdisciplinary Sciences, Tohoku University, Sendai, Miyagi 980-8578, Japan*

Accepted XXX. Received YYY; in original form ZZZ

## ABSTRACT

Dust enables low-mass stars to form from low-metallicity gas by inducing fragmentation of clouds via the cooling by its thermal emission. Dust may, however, be evacuated from star-forming clouds due to radiation force from massive stars. We here study the condition for the dust evacuation by comparing the dust evacuation time with the time of cloud destruction due to either expansion of HII regions or supernovae. The cloud destruction time has weak dependence on the cloud radius, while the dust evacuation time becomes shorter for a cloud with the smaller radius. The dust evacuation thus occurs in compact star-forming clouds whose column density is  $N_{\text{H}} \simeq 10^{24} - 10^{26} \text{ cm}^{-2}$ . The critical halo mass above which the dust evacuation occurs becomes lower for higher formation redshift, e.g.,  $\sim 10^9 M_{\odot}$  at redshift  $z \sim 3$  and  $\sim 10^7 M_{\odot}$  at  $z \sim 9$ . In addition, metallicity of the gas should be less than  $\sim 10^{-2} Z_{\odot}$ . Otherwise the dust attenuation reduces the radiation force significantly. From the dust-evacuated gas, massive stars are likely to form even with metallicity above  $\sim 10^{-5} Z_{\odot}$ , the critical value for low-mass star formation due to the dust cooling. This can explain the dearth of ultra-metal poor stars with the metallicity lower than  $\sim 10^{-4} Z_{\odot}$ .

**Key words:** stars: formation – stars: Population II – stars: low-mass – galaxies: evolution – dust, extinction

## 1 INTRODUCTION

The initial mass function (IMF) of stars deeply influences subsequent galaxy evolution and star formation history. Stellar feedback from massive stars alter the physical state and structure of the interstellar medium (e.g. McKee & Ostriker 1977). Supernovae (SNe) provide the interstellar medium with heavy elements and foster chemical evolution of galaxies. On the other hand, low mass stars account for the most of stellar mass of aged galaxies due to their longevity. Even primordial low-mass stars, if formed, can still survive as main sequence stars in the Galaxy (e.g. Machida et al. 2008; Clark et al. 2011).

The mass of stars likely depends on the metallicity of the forming environments. At the solar metallicity, the IMF has the peak around  $0.4 M_{\odot}$ , which means the most stars are low-mass objects (Kroupa 2001; Chabrier 2003). On the other hand, the IMF of primordial stars was theoretically predicted with recent radiative-hydrodynamics simulations in the cosmological context. (Hirano et al. 2014, 2015; Susa et al. 2014; Stacy et al. 2016; Hosokawa et al. 2016). Those numerical simulations suggest that the primordial stars were

formed in the mass range in  $\sim 10 M_{\odot}$  - a few  $100 M_{\odot}$  with the typical mass being much larger than that of the sun.

This transition in the characteristic stellar mass from massive to low-mass objects can be ascribed to the change in fragmentation mass of star-forming clumps with accumulation of metals (Omukai 2000; Bromm et al. 2001). In literatures, the transitional metallicity is often called the critical metallicity  $Z_{\text{crit}}$ . Fragmentation of clumps is induced by the dust cooling (Schneider et al. 2002) as well as metal-line cooling (Bromm et al. 2001). With gas-phase metals, clumps fragment into massive dense cores of no smaller than a few  $10 M_{\odot}$  even with  $Z \gtrsim 10^{-3.5} Z_{\odot}$  (Bromm & Loeb 2003; Santoro & Shull 2006). On the other hand, the fragmentation mass becomes as small as  $0.1 - 1 M_{\odot}$  in the case of taking into account the dust cooling for  $Z \gtrsim 10^{-6} - 10^{-5} Z_{\odot}$  (Omukai et al. 2005; Schneider et al. 2003) in the case that the dust depletion factor, which is defined by

$$f_{\text{dep}} \equiv \frac{M_{\text{dust}}}{M_{\text{dust}} + M_{\text{metal}}}, \quad (1)$$

where  $M_{\text{metal}}$  is the metal mass in the gas phase and  $M_{\text{dust}}$  is that taken into dust grains, is the same as in the Galaxy. By converting this metallicity into dust-to-gas ratio  $\mathcal{D}$ , the critical dust-to-gas ratio is  $\mathcal{D}_{\text{crit}} = [2.6 - 6.3] \times 10^{-9}$  (Schneider et al. 2012). Therefore, the dust cooling is supposed to pro-

\* E-mail: fukushima@tap.scphys.kyoto-u.ac.jp

duce low-mass stars of  $\lesssim 1 M_{\odot}$  even at such low metallicity as  $10^{-6} - 10^{-5} Z_{\odot}$ .

Recent survey observations successfully discovered several metal-poor stars with metallicity lower than  $\sim 10^{-4} Z_{\odot}$ , but these ultra-metal poor stars are very rare in the Galaxy (e.g. [Frebel & Norris 2015](#)). [Salvadori et al. \(2007\)](#) indicated that the threshold of metallicity for the formation of low-mass stars should be  $\sim 10^{-4} Z_{\odot}$  in order to reproduce the metallicity distribution of observed metal-poor stars in the Galactic halo. This value does not coincide with the theoretical expectation for the critical metallicity for dust-induced fragmentation,  $Z_{\text{crit}} = 10^{-6} - 10^{-5} Z_{\odot}$ .

This discrepancy can be alleviated by reducing the dust depletion factor in low-metallicity environments. Namely, if the dust depletion factor is smaller than in the solar neighborhood,  $\mathcal{D}$  may still fall short of  $\mathcal{D}_{\text{crit}}$  even for the gas with nominal metallicity higher than  $Z_{\text{crit}}$ .

One way to reduce  $f_{\text{dep}}$  is slower growth of dust mass in low-metallicity interstellar medium (e.g., [Asano et al. 2013](#)). Recently [Rémy-Ruyer et al. \(2014\)](#) suggested that the observed lower dust depletion factor in the low-metallicity galaxies in the local universe could be explained by such mechanism.

Another possible mechanism, which we focus on in this paper, is the dust evacuation from star-forming regions caused by radiation feedback from massive stars. In this case, dust grains are pushed out due to the radiation force and can be decoupled from the gas component. In fact, the lower amount of dust grains in the observed HII regions around massive stars than in the HI gas is likely to be caused by such mechanism ([Draine 2011a](#); [Akimkin et al. 2015, 2017](#); [Ishiki et al. 2018](#)). Also, the radiation force has been claimed to be able to expel dust grains even from galactic haloes ([Chiao & Wickramasinghe 1972](#); [Ferrara et al. 1991](#)). Similarly, we speculate that the dust evacuation also occurs in low-metallicity star-forming clouds in the early universe, thereby allowing massive star formation to continue even with certain metal enrichment.

In this paper, we study the condition for the formation of dust-free star-forming clouds as a result of dust evacuation by the radiation force. We have found that the dust evacuation successfully occurs in clouds with high column density  $N_{\text{H}} \simeq 10^{24} - 10^{26} \text{ cm}^{-2}$  and very low metallicity  $Z \lesssim 10^{-2} Z_{\odot}$ . In terms of galaxy properties, this occurs more easily for higher halo mass and formation redshift, e.g., halos of  $\sim 10^9 M_{\odot}$  ( $\sim 10^7 M_{\odot}$ ) at  $z \sim 3$  ( $z \sim 9$ , respectively), as long as very low-metallicity gas is available.

We organize the rest of the paper as follows. In Section 2, we first consider the dust evacuation from a homogeneous spherical star-forming cloud. We then estimate the conditions for the dust evacuation from a galactic disk in Section 3. In Section 4, we investigate the possible effects that inhibit the dust evacuation. Finally, we summarize our results and give discussions in Section 5. The effect of the Coulomb drag force on the terminal velocity of grains is described in Appendix A.

## 2 DUST GRAIN EVACUATION FROM A STAR FORMING CLOUD

### 2.1 Formation efficiency and radiation emissivity of star clusters

We first consider the simplest case of spherical and uniform density star-forming clouds. For a cloud with the mass  $M_{\text{cl}}$ , radius  $R_{\text{cl}}$  and star formation efficiency (SFE)  $\epsilon_*$ , the total stellar mass  $M_*$  formed in the cloud is given by

$$M_* = \epsilon_* M_{\text{cl}} = 10^5 M_{\odot} \left( \frac{\epsilon_*}{0.1} \right) \left( \frac{M_{\text{cl}}}{10^6 M_{\odot}} \right). \quad (2)$$

The SFE  $\epsilon_*$  is likely to depend on the properties of star-forming clouds ([Katz 1992](#)). Here we estimate the growth rate of the total stellar mass based on the local free-fall time  $t_{\text{ff}}$  as

$$\frac{dM_*}{dt} = c_* \frac{M_{\text{cl}} - M_*}{t_{\text{ff}}}, \quad (3)$$

where  $c_*$  is a parameter characterizing the star formation rate (SFR), and  $t_{\text{ff}}$  is defined as

$$t_{\text{ff}} = \sqrt{\frac{3\pi}{32Gm_{\text{H}}n_{\text{H}}}}, \quad (4)$$

where the number density of gas  $n_{\text{H}}$  is given as

$$n_{\text{H}} = \frac{M_{\text{cl}}}{\frac{4}{3}\pi R_{\text{cl}}^3 m_{\text{H}}} = 9.7 \times 10^3 \text{ cm}^{-3} \left( \frac{R_{\text{cl}}}{10 \text{ pc}} \right)^{-3} \left( \frac{M_{\text{cl}}}{10^6 M_{\odot}} \right). \quad (5)$$

We estimate the total stellar mass  $M_*$  by integrating Equation (3) with the condition  $M_* = 0$  at  $t = 0$ :

$$M_* = M_{\text{cl}} \left[ 1 - \exp\left(-c_* \frac{t}{t_{\text{ff}}}\right) \right]. \quad (6)$$

Massive stars are expected to end their lives as SNe. Their feedback likely destroys the star-forming clouds and stops further star formation. In addition, newly formed dust grains will be supplied in those events. Therefore, we use the SFE at the lifetime of OB stars,  $t = t_{\text{OB}}$ , in estimating the condition for the dust evacuation:

$$\epsilon_* = \left[ 1 - \exp\left(-c_* \frac{t_{\text{OB}}}{t_{\text{ff}}}\right) \right]. \quad (7)$$

The relation among  $\epsilon_*$ ,  $M_{\text{cl}}$ ,  $R_{\text{cl}}$  and  $c_*$  is shown in Figure 1. For  $M_{\text{cl}} = 10^6 M_{\odot}$ ,  $R_{\text{cl}} = 10 \text{ pc}$ , the SFE becomes  $\epsilon_* = 0.38$  ( $4.7 \times 10^{-2}$ ) for  $c_* = 0.1$  (0.01, respectively).

We use the IMF  $\psi(m_*)$  of [Larson \(1998\)](#):

$$\psi(m_*) = \frac{dN}{d \log m_*} \propto \left( 1 + \frac{m_*}{m_{\text{ch}}} \right)^{-1.35}, \quad (8)$$

where  $m_{\text{ch}}$  is the characteristic stellar mass formed. In this paper, we consider the case of  $m_{\text{ch}} = 10 M_{\odot}$  as the fiducial one, which is claimed by [Komiya et al. \(2007\)](#) based on the carbon enhanced metal-poor (CEMP) star statistics in the Galaxy. We also study the cases with low stellar mass  $m_{\text{ch}} = 1 M_{\odot}$  as in the solar neighborhood (e.g., [Kroupa 2001](#)), and very massive stars  $m_{\text{ch}} = 50 M_{\odot}$  as in the primordial star formation ([Hosokawa et al. 2011](#)). We take the mass range from  $0.1 M_{\odot}$  to  $300 M_{\odot}$  in all the cases.

Next, we estimate the total luminosity  $L_{\text{tot}}$  and the total ionizing photon emissivity  $S_{\text{tot}}$  of a star cluster. We use the stellar isochrone calculated by [Chen et al. \(2015\)](#) with metallicity  $Z = 10^{-2} Z_{\odot}$  and at  $t = 10^6 \text{ yr}$  roughly corresponding

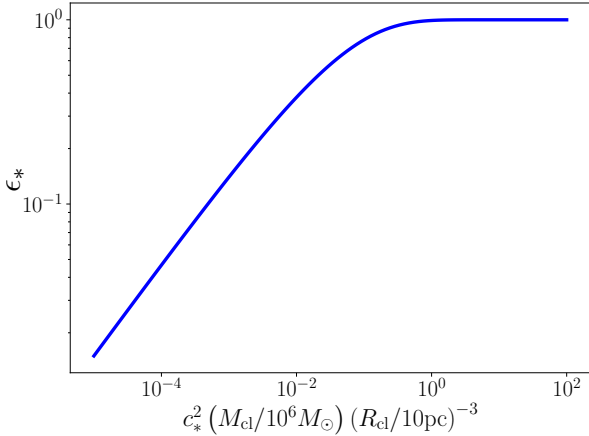


**Figure 1.** The SFE  $\epsilon_*$  as a function of the cloud mass  $M_{\text{cl}}$ , the cloud radius  $R_{\text{cl}}$  and  $c_*$  (Eq. 7). We used  $t_{\text{OB}} = 2.5 \times 10^6 \text{ yr}$ .

**Table 1.** The luminosity and the ionizing photon emissivity per unit stellar mass for different characteristic stellar mass  $m_{\text{ch}}$ . The numbers are in unit of ( $L_{\odot} M_{\odot}^{-1}$ ) and ( $\text{s}^{-1} M_{\odot}^{-1}$ ).

$m_{\text{ch}} [M_{\odot}]$	$\langle L_*/m_* \rangle$	$\langle S_*/m_* \rangle$
1	$2.9 \times 10^3$	$2.2 \times 10^{47}$
10	$6.7 \times 10^3$	$5.0 \times 10^{47}$
50	$1.1 \times 10^4$	$8.3 \times 10^{47}$

to half the average cloud lifetime. Figure 2 illustrates the luminosity  $L_*(m_*)$ , the effective temperature  $T_{\text{eff}}(m_*)$ , and the ionizing photon emissivity  $S_*$  as functions of the stellar mass. The luminosity and the ionizing photon emissivity per unit stellar mass are calculated by taking the average with the weight of the IMF (Eq. 8). They are presented in Table 1. In the fiducial case with  $m_{\text{ch}} = 10 M_{\odot}$ , the total luminosity and ionization emissivity are

$$L_{\text{tot}} = 6.7 \times 10^8 L_{\odot} \left( \frac{\epsilon_*}{0.1} \right) \left( \frac{M_{\text{cl}}}{10^6 M_{\odot}} \right), \quad (9)$$

and

$$S_{\text{tot}} = 5.0 \times 10^{52} \text{ s}^{-1} \left( \frac{\epsilon_*}{0.1} \right) \left( \frac{M_{\text{cl}}}{10^6 M_{\odot}} \right). \quad (10)$$

## 2.2 Dust evacuation time

The motion of dust grains is governed by three forces: radiation force  $F_{\text{rad}}$ , gravity  $F_{\text{grav}}$  and drag force  $F_{\text{drag}}$ . We estimate the dust terminal velocity  $v_{\text{d}}$  as follows.

Radiation force  $F_{\text{rad}}$  exerted on a dust grain is

$$F_{\text{rad}} = \frac{\pi a^2 Q L_{\text{tot}}}{4\pi r^2 c}, \quad (11)$$

where  $a$  is the radius of the dust grain and  $Q$  is the absorption efficiency factor relative to the geometrical cross section. The efficiency factor  $Q$  depends on the size of dust grains and the frequency of radiation. When the cloud is optically thin, radiation field inside the cloud is dominated by the direct light from massive stars, which can be approximated by the black-body spectrum of  $\sim 2 \times 10^4$  K. On the other hand,

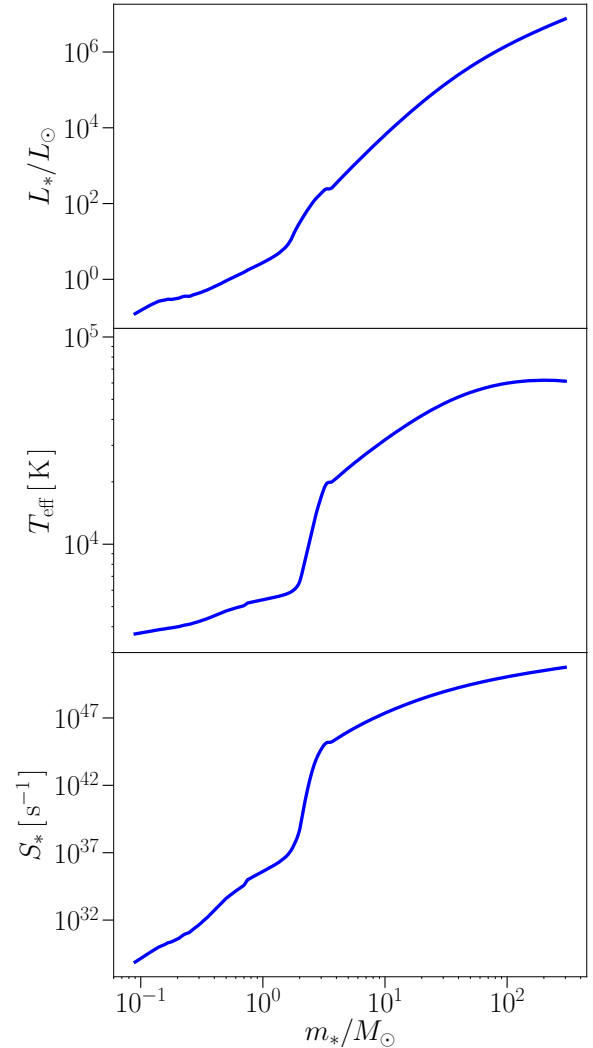


**Figure 2.** The luminosity  $L_*$  (top), the effective temperature  $T_{\text{eff}}$  (middle) and ionizing photon emissivity  $S_*$  (bottom) of stars at metallicity  $10^{-2} Z_{\odot}$  and  $t = 10^6$  yr as a function of their mass (Chen et al. 2015).

in the optically thick case the stellar light is absorbed and re-emitted by dust grains, and the radiation is dominated by the diffuse light, which is roughly the black body of  $\sim 100$  K (e.g., Fukushima et al. 2018). Figure 3 shows the size dependence of the efficiency factor  $Q$  of graphite and silicate grains both for the direct and diffuse light. Note  $Q \approx 1$  ( $\approx 10^{-2}$ ) for the direct (diffuse, respectively) light for grains with  $a \approx 0.1 \mu\text{m}$ .

The ratio of radiation force to the gravity on a dust grain is

$$\begin{aligned} \frac{F_{\text{rad}}}{F_{\text{grav}}} &= \frac{\pi a^2 Q L_{\text{tot}}}{4\pi c G M_{\text{cl}} m_{\text{d}}} \\ &= 1.3 \times 10^3 \left( \frac{Q}{1} \right) \left( \frac{\rho_{\text{d}}}{3 \text{ g cm}^{-3}} \right)^{-1} \left( \frac{a}{0.1 \mu\text{m}} \right)^{-1} \left( \frac{\epsilon_*}{0.1} \right). \end{aligned} \quad (12)$$

That is, the gravity is negligible compared to the radiation

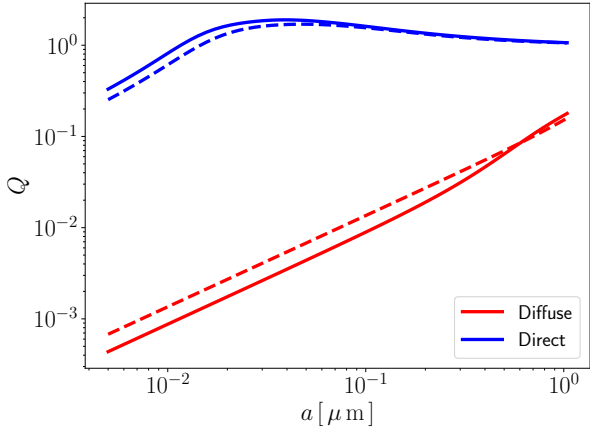


**Figure 3.** The absorption efficiency factor  $Q$  to geometric area as a function of dust size. Blue and red lines show the values to the stellar radiation of black body with the effective temperature of  $2 \times 10^4$  K and the diffuse thermal emission of dust with the temperature of 100 K, respectively. The solid- and dashed-lines represent graphite and silicate dust grains. We calculate the efficiency factor  $Q$  from Mie theory with the dielectric function of [Draine & Lee \(1984\)](#) and [Draine \(2003\)](#).

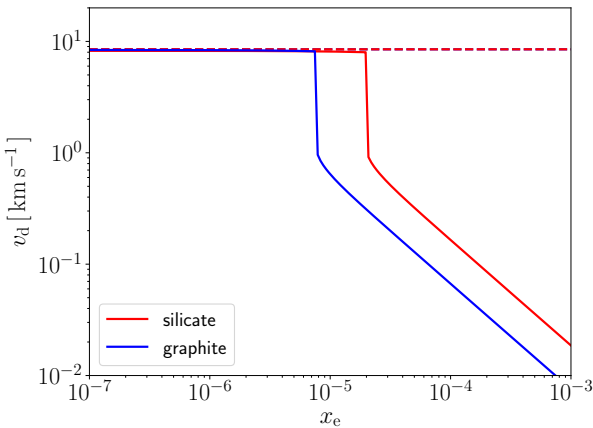


**Figure 4.** The terminal velocity of dust grains in a star-forming cloud  $M_{\text{cl}} = 10^6 M_{\odot}$ ,  $R_{\text{cl}} = 10$  pc and  $\epsilon_* = 0.1$ . The solid and dashed lines show the velocities estimated with and without Coulomb drag force, respectively. The blue and red lines are for the graphite and silicate grains, respectively.

force. The terminal velocity of dust  $v_d$  is determined by the balance between radiation and drag forces alone.

We consider the collisional gas drag  $F_{\text{collision}}$  and the Coulomb drag  $F_{\text{Coulomb}}$  as the drag force on dust grains,  $F_{\text{drag}} = F_{\text{collision}} + F_{\text{Coulomb}}$  (see Appendix A for the expression). The Coulomb drag and thus the relative velocity of dust grains sensitively depend on the ionization degree  $x_e$  in the cloud (for the estimation of the terminal velocity, see Appendix A). Figure 4 shows the terminal velocity of a dust grain with  $0.1 \mu\text{m}$  as a function of ionization degree for the cloud with  $M_{\text{cl}} = 10^6 M_{\odot}$ ,  $R_{\text{cl}} = 10$  pc and  $\epsilon_* = 0.1$ . The

solid lines show the terminal velocities calculated by considering both the collisional and Coulomb drag forces, while the dashed lines are those with the collisional drag force alone. For  $x_e \gtrsim 10^{-5}$ , the Coulomb drag dominates the collisional drag, and the velocity of dust grains suddenly falls below  $1 \text{ km s}^{-1}$ . In contrast, the Coulomb drag does not work for  $x_e \lesssim 10^{-5}$ , and the terminal velocity is  $\sim 10 \text{ km s}^{-1}$ , set by the collisional drag.

In our model, free electrons are supplied by the ionization either of heavy elements by far ultraviolet (FUV) light or of hydrogen by cosmic rays. The typical number density  $n(\text{M}^+)$  of heavy elements ionized by FUV photons of  $h\nu < 13.6\text{eV}$  in HI regions is estimated by [Draine \(2011b\)](#) as

$$x_{\text{M}} = n(\text{M}^+)/n_{\text{H}} \simeq 1.1 \times 10^{-4} \quad (13)$$

for the solar metallicity gas. Therefore, in the low-metallicity case of  $Z \lesssim 10^{-1} Z_{\odot}$ , we expect that  $x_{\text{M}} \lesssim 10^{-5}$  and thus the Coulomb drag can be neglected. The hydrogen ionization fraction by cosmic rays is calculated by the balance between the ionization rate of cosmic rays  $\xi_{\text{CR}}$  and the recombination rate of ionized hydrogen,

$$n_{\text{H}} \xi_{\text{CR}} = \alpha_{\text{B}} n_{\text{H}}^2 x_{\text{e}}^2, \quad (14)$$

where  $\alpha_{\text{B}}$  is the case-B recombination coefficient. Thus,  $x_e$  is given as,

$$\begin{aligned} x_e &= \left( \frac{\xi_{\text{CR}}}{\alpha_{\text{B}} n_{\text{H}}} \right)^{1/2} \\ &= 3.8 \times 10^{-5} \left( \frac{\xi_{\text{CR}}}{10^{-16} \text{s}^{-1}} \right)^{1/2} \left( \frac{R_{\text{cl}}}{10 \text{ pc}} \right)^{3/2} \left( \frac{M_{\text{cl}}}{10^6 M_{\odot}} \right)^{-1/2}, \end{aligned} \quad (15)$$

where we have used  $\alpha_{\text{B}} = 7 \times 10^{-12} \text{ cm}^3 \text{ s}^{-1}$  at  $T = 100$  K ([Hummer & Storey 1987](#)). Ionized hydrogen also recombines via the charge exchange reactions with heavy elements (e.g. CO) and the ionization fraction becomes smaller than  $10^{-6}$  for number density higher than  $\sim 10^3 \text{ cm}^{-3}$  ([McKee 1989](#)). Thus Equation (15) gives the upper limit of ionization degree, which is likely to be smaller than the critical value above which the Coulomb drag becomes important. Therefore, we ignore the Coulomb drag below and estimate the dust terminal velocity from the balance between the collisional drag and radiation forces. Here, we only consider the cosmic rays as the ionization source. In section 4.1, we discuss the effects of other sources, such as X-rays or mixing of ionized and neutral gases.

For supersonic relative velocity between the gas and dust, the collisional drag force can be written as  $F_{\text{collision}} = \pi a^2 v_{\text{d}}^2 n_{\text{H}} m_{\text{H}}$  ([Draine & Salpeter 1979](#)). The terminal velocity  $v_d$  is then given as

$$\begin{aligned} v_d &= \sqrt{\frac{L_{\text{tot}} Q}{4\pi R_{\text{cl}}^2 c n_{\text{H}} m_{\text{H}}}} \\ &= 6.7 \text{ km s}^{-1} \left( \frac{Q}{1} \right)^{1/2} \left( \frac{\epsilon_*}{0.1} \right)^{1/2} \left( \frac{R_{\text{cl}}}{10 \text{ pc}} \right)^{1/2}. \end{aligned} \quad (16)$$

Dust evacuation time  $t_{\text{evac}}$  from a star-forming cloud is esti-

mated as

$$\begin{aligned}
 t_{\text{evac}} &= \frac{R_{\text{cl}}}{v_{\text{d}}} \\
 &= \sqrt{\frac{4\pi c n_{\text{H}} m_{\text{H}}}{L_{\text{tot}} Q}} R_{\text{cl}}^2 \\
 &= 1.5 \times 10^6 \text{ yr} \left(\frac{Q}{1}\right)^{-1/2} \left(\frac{\epsilon_*}{0.1}\right)^{-1/2} \left(\frac{R_{\text{cl}}}{10 \text{ pc}}\right)^{1/2}. \quad (17)
 \end{aligned}$$

Note that  $t_{\text{evac}}$  increases with the cloud radius.

Note that the drag time  $t_{\text{drag}}$  required for transporting momentum from a grain to the gas is given as

$$\begin{aligned}
 t_{\text{drag}} &= \frac{m_{\text{d}} v_{\text{d}}}{F_{\text{drag}}} \\
 &= 1.2 \times 10^2 \text{ yr} \left(\frac{Q}{1}\right)^{-1/2} \left(\frac{\rho_{\text{d}}}{3 \text{ g cm}^{-3}}\right) \\
 &\quad \times \left(\frac{a}{0.1 \mu\text{m}}\right) \left(\frac{\epsilon_*}{0.1}\right)^{-1/2} \left(\frac{R_{\text{cl}}}{10 \text{ pc}}\right)^{5/2} \left(\frac{M_{\text{cl}}}{10^6 M_{\odot}}\right)^{-1}, \quad (18)
 \end{aligned}$$

which is much shorter than the evacuation time  $t_{\text{evac}}$  (Eq. 17). Therefore, our use of the terminal velocity as the dust velocity is justified.

In estimating  $t_{\text{evac}}$ , we have used the efficiency factor of  $Q = 1$  corresponding to the optically thin case. If the cloud is optically thick, on the other hand, the radiation force on to dust grains is imparted mostly by the diffuse light and the efficiency factor drops to  $Q = 10^{-2}$ . With such low efficiency factor, the dust evacuation time (Eq. 17) becomes as long as  $t_{\text{evac}} = 1.5 \times 10^7 \text{ yr}$ , exceeding the lifetime of massive stars  $t_{\text{OB}}$ . Thus, optically-thick clouds would be destructed or replenished with newly formed dust grains due to the SN feedback before dust grains are evacuated. Therefore, the clouds must be optically thin initially to become dust-free by the dust evacuation. Using the dust opacity  $\kappa = 350 \text{ cm}^2 \text{ g}^{-1} (Z/Z_{\odot})$  at the wavelength  $\lambda_{\text{max}} = 0.254 \mu\text{m}$ , which is the peak of the black body spectrum of  $T = 2 \times 10^4 \text{ K}$ , we estimate the optical depth of the cloud as

$$\begin{aligned}
 \tau &= \rho \kappa R_{\text{cl}} \\
 &= 175 \left(\frac{\kappa}{350 \text{ cm}^2 \text{ g}^{-1}}\right) \left(\frac{R_{\text{cl}}}{10 \text{ pc}}\right)^{-2} \left(\frac{M_{\text{cl}}}{10^6 M_{\odot}}\right) \left(\frac{Z}{Z_{\odot}}\right). \quad (19)
 \end{aligned}$$

The condition for optical thinness thus corresponds to metallicity

$$Z < 5.7 \times 10^{-3} Z_{\odot} \left(\frac{\kappa}{350 \text{ cm}^2 \text{ g}^{-1}}\right)^{-1} \left(\frac{R_{\text{cl}}}{10 \text{ pc}}\right)^2 \left(\frac{M_{\text{cl}}}{10^6 M_{\odot}}\right)^{-1}. \quad (20)$$

In the estimation above, we do not consider the dust size dependence of the efficiency factor and always use the value  $Q = 1$ . As seen in Figure 3, this is only true for grains larger than  $\sim 0.01 \mu\text{m}$ . For grains smaller than  $0.01 \mu\text{m}$ , the efficiency factor becomes  $Q \lesssim 0.3$ , which makes the evacuation time longer due to the weaker radiation force. In fact, by substituting  $Q = 0.3$  into Equation (17), dust evacuation time becomes  $t_{\text{evac}} = 2.7 \times 10^6 \text{ yr}$ , slightly exceeding  $t_{\text{OB}}$ . In this case, small grains with size  $a < 0.01 \mu\text{m}$  would remain in the cloud. In Section 4.2, we additionally discuss cases in which small dust grains are dominant. The dependence of timescales on the grain size is discussed in Appendix A.

### 2.3 Cloud lifetime

For star formation from the dust-free gas, dust evacuation time must to be shorter than destruction time of the cloud. Lifetime of the star-forming cloud  $t_{\text{cl}}$  is estimated with the timescale that either type-II SNe occur  $t_{\text{OB}}$  or the ionizing front reaches the boundary of the cloud  $t_{\text{HII}}$ :

$$t_{\text{cl}} = \min(t_{\text{OB}}, t_{\text{HII}}). \quad (21)$$

The timescale of SNe is determined by the lifetime of massive stars, and we use  $t_{\text{OB}} = 2.5 \times 10^6 \text{ yr}$ , which is the lifetime for  $m_* = 120 M_{\odot}$  (Schaerer 2002), in this work.

The expansion time of an HII region  $t_{\text{HII}}$  can be calculated as follows. The ionizing front reaches the Strömgen radius

$$\begin{aligned}
 R_{\text{S0}} &= \left(\frac{3S_{\text{tot}}}{4\pi n_{\text{H}}^2 \alpha_{\text{B}}}\right)^{1/3} \\
 &= 2.5 \text{ pc} \left(\frac{\epsilon_*}{0.1}\right)^{1/3} \left(\frac{R_{\text{cl}}}{10 \text{ pc}}\right)^2 \left(\frac{M_{\text{cl}}}{10^6 M_{\odot}}\right)^{-1/3}, \quad (22)
 \end{aligned}$$

almost instantly in a few hundred years or so. Here, we have used Equation (10) for number density of gas and case-B recombination rate  $\alpha_{\text{B}} = 2.6 \times 10^{-13} \text{ cm}^3 \text{ s}^{-1}$  (at  $T = 10^4 \text{ K}$ , Osterbrock & Ferland 2006). Thereafter the pressure imbalance drives the further expansion of the HII region. The radius of the HII region in this phase is given by (Spitzer 1978)

$$R_{\text{HII}} = R_{\text{S0}} \left[1 + \frac{7}{4} \frac{c_{\text{HII}} t}{R_{\text{S0}}}\right]^{4/7}. \quad (23)$$

By equating  $R_{\text{HII}}$  with the cloud radius  $R_{\text{cl}}$ , we obtain the time for HII region to reach the cloud boundary:

$$\begin{aligned}
 t_{\text{HII}} &= \frac{4}{7} \frac{R_{\text{S0}}}{c_{\text{HII}}} \left[ \left(\frac{R_{\text{cl}}}{R_{\text{S0}}}\right)^{7/4} - 1 \right] \\
 &\approx 1.4 \times 10^6 \text{ yr} \left(\frac{\epsilon_*}{0.1}\right)^{-1/4} \left(\frac{R_{\text{cl}}}{10 \text{ pc}}\right)^{1/4} \left(\frac{M_{\text{cl}}}{10^6 M_{\odot}}\right)^{1/4}. \quad (24)
 \end{aligned}$$

In the numerical estimate above, we have used the temperature in the HII region  $T = 10^4 \text{ K}$  and the sound speed  $c_{\text{HII}} = 11.4 \text{ km s}^{-1}$ . Note that the expansion time of HII region has weak dependence on the cloud radius compared with the dust evacuation time (Eq. 17).

We now examine whether the radiation force on the dust destroys the star-forming cloud itself. Since the ratio of radiation force to the gravity at  $R_{\text{cl}}$  is

$$\begin{aligned}
 \frac{F_{\text{rad}}}{F_{\text{grav}}} &= \frac{\kappa_{\text{d}} L_*}{4\pi c G M_{\text{cl}}} \\
 &= 1.8 \times 10^{-2} \left(\frac{\kappa}{350 \text{ cm}^2 \text{ g}^{-1}}\right) \left(\frac{\epsilon_*}{0.1}\right) \left(\frac{Z}{10^{-3} Z_{\odot}}\right), \quad (25)
 \end{aligned}$$

the radiation force is smaller than gravity on the gas component in optically-thin clouds. Such clouds can avoid being disrupted by the radiation force.

### 2.4 The condition for dust-free cloud formation

We here obtain the condition for formation of the dust-free star-forming clouds. In order for stars to form from the dust-free gas, the dust evacuation time be shorter than the

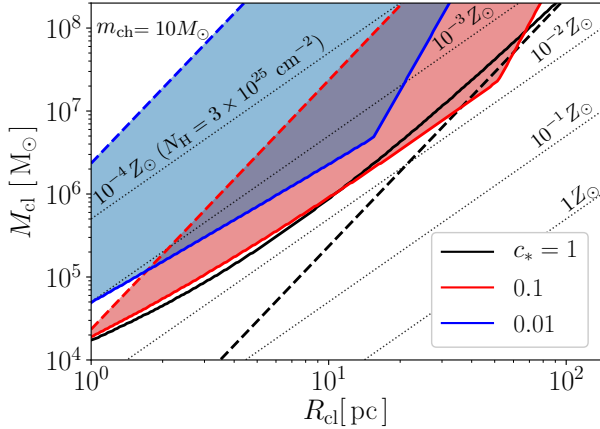


**Figure 5.** The conditions for the formation of dust-free star-forming clouds in the case of  $m_{\text{ch}} = 10 M_{\odot}$ . The black, red, and blue solid lines denote the condition of  $t_{\text{evac}} < t_{\text{cl}}$  in the cases with  $c_* = 1, 0.1$  and  $0.01$ , respectively. Above the dashed line, SFE becomes  $\epsilon_* > 0.9$ . The blue and red shaded regions represent that the dust evacuation occurs and more than 10 per cent of initial gas remains at this epoch. In the case with  $c_* = 1$ , there is no such area. The black-dot lines show the boundaries at where the optical depth becomes  $\tau = 1$  at each metallicity, and clouds are optically thin below these lines. The relation for  $\tau = 1$  between the column density  $N_{\text{H}}$  and metallicity  $Z$  is denoted as  $N_{\text{H}} = 3 \times 10^{25} \text{ cm}^{-2} (Z/10^{-4} Z_{\odot})$ .

cloud lifetime  $t_{\text{cl}}$ , and also some gas still be available at this moment for subsequent star formation.

We consider the cases with the star-formation rate parameter  $c_* = 0.01 - 1$ , which is related to the SFE  $\epsilon_*$  by Equation (7). Figure 5 shows the condition for the formation of a dust-free star-forming cloud in the case with the characteristic stellar mass  $m_{\text{ch}} = 10 M_{\odot}$ . The color-shaded areas show the parameter ranges of clouds that become dust-free for different values of  $c_*$ . The black, red and blue lines correspond to the cases with  $c_* = 1, 0.1$ , and  $0.01$ , respectively. The condition of the optical depth  $\tau = 1$  is also shown by the thin dotted lines for indicated metallicities, and the clouds are optically thin below them. For smaller  $c_*$ , the dust evacuation time  $t_{\text{evac}}$  becomes longer from Equation (17) and the clouds must be more compact for the dust evacuation. The SFE  $\epsilon_*$  is larger than 0.9 above the dashed lines in Figure 5. In these regions, most of the gas has been consumed by star formation by the time of the dust evacuation. As a result, star formation from the dust-free gas is only realized in the color-shaded areas between the solid and dashed-lines. In the case with  $c_* = 1$ , there is no shaded area, which means that star formation from the dust-free gas does not occur in any clouds below  $10^8 M_{\odot}$ . In the case with  $c_* = 0.1$ , this condition roughly corresponds to the column density  $10^{24} \text{ cm}^{-2} \lesssim N_{\text{H}} \lesssim 10^{25} \text{ cm}^{-2}$  and the metallicity  $Z \lesssim 10^{-2} Z_{\odot}$ . Also, in the case with  $c_* = 0.01$ , the condition becomes  $3 \times 10^{24} \text{ cm}^{-2} \lesssim N_{\text{H}} \lesssim 10^{26} \text{ cm}^{-2}$  and  $Z \lesssim 10^{-3} Z_{\odot}$ . Namely, in compact and low-metallicity clouds, the dust evacuation is likely to occur. Comparing this value with the column density of local giant molecular clouds (GMCs)  $N_{\text{H}} \approx 10^{22} \text{ cm}^{-2}$  (Solomon et al. 1987) or OB star-forming clumps  $N_{\text{H}} \approx 10^{24} \text{ cm}^{-2}$  (Plume et al. 1997), the dust evac-

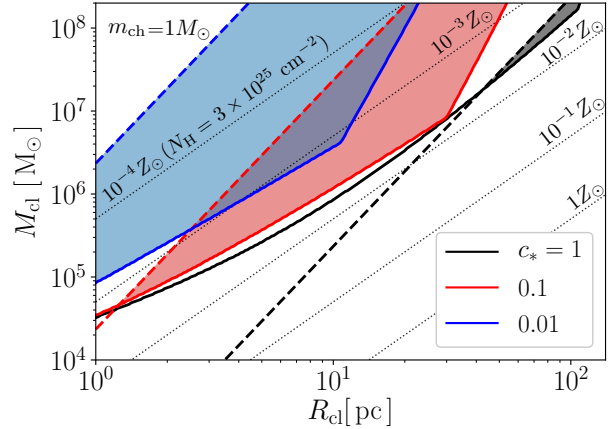


**Figure 6.** Same as Figure 5, but for the case of lower characteristic stellar mass  $m_{\text{ch}} = 1 M_{\odot}$ . In this case, the dust-free star formation condition is satisfied also for  $c_* = 1$  in a very narrow strip with  $\gtrsim 10^7 M_{\odot}$ .

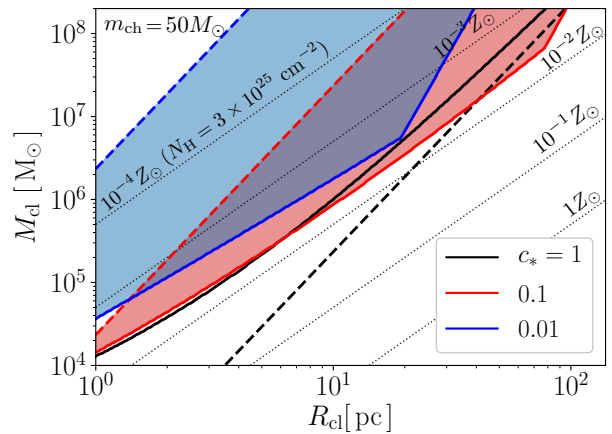


**Figure 7.** Same as Figure 5, but for the case of higher characteristic stellar mass  $m_{\text{ch}} = 50 M_{\odot}$ .

uation does not occur in typical GMCs, while it is satisfied in local massive star-forming clumps if the metallicity were low enough. The cases with different characteristic stellar mass  $m_{\text{ch}} = 1$  and  $50 M_{\odot}$  are shown in Figures 6 and 7, respectively. For higher  $m_{\text{ch}}$ , the luminosity per unit mass becomes higher (Table 1), which facilitates the dust evacuation and thus results in the wider shaded regions, and vice versa. The condition on  $(M_{\text{cl}}, R_{\text{cl}})$  for the dust evacuation, however, does not depend so much on the value of  $m_{\text{ch}}$ .

As a rule of thumb, for star formation from the dust evacuated gas to occur, the clouds should be massive or compact  $N_{\text{H}} \approx 10^{24} - 10^{26} \text{ cm}^{-2}$ , and low-metallicity  $Z \lesssim 10^{-2} Z_{\odot}$ . In addition, the SFR parameter must be somewhat smaller than unity.

### 3 DUST EVACUATION FROM GALACTIC DISKS

We have studied the dust evacuation from spherical star-forming clouds. In this section, by applying the model developed in Section 2, we study the dust evacuation from disk-like structure likely to form in low-metallicity galaxies in the early universe.

#### 3.1 Galactic disk model

We consider a halo with mass  $M_h$  virializing at redshift  $z_{\text{vir}}$  and a rotationally-supported disk within it (Mo et al. 1998; Oh & Haiman 2002). The virial radius is given by

$$R_{\text{vir}} = 2.2 \text{kpc} \left( \frac{1+z_{\text{vir}}}{10} \right)^{-1} \left( \frac{M_h}{10^9 M_\odot} \right)^{1/3}. \quad (26)$$

Using the spin parameter  $\lambda = J|E|^{1/2}/GM_h^{5/2}$ , where  $E$  and  $J$  are the total energy and the total angular momentum of the halo, the disk radius is estimated as

$$R_d = \frac{\lambda}{\sqrt{2}} R_{\text{vir}} = 77 \text{pc} \left( \frac{\lambda}{0.05} \right) \left( \frac{1+z_{\text{vir}}}{10} \right)^{-1} \left( \frac{M_h}{10^9 M_\odot} \right)^{1/3}. \quad (27)$$

The number density of the gas at radius  $r$  and vertical height  $z$  is

$$n(r, z) = n_0 \exp\left(-\frac{2r}{R_d}\right) \text{sech}^2\left(\frac{z}{\sqrt{2}z_0}\right), \quad (28)$$

where  $z_0$  is the vertical scale height,

$$z_0 = \frac{c_s}{4\pi G \mu m_H n_0} e^{r/R_d}. \quad (29)$$

We set the mean molecular weight  $\mu = 1$ . Note that the disk mass can be written as

$$M_d = \int dz \int 2\pi r dr \mu m_H n(r, z) = f_d (\Omega_b / \Omega_m) M_h, \quad (30)$$

where  $f_d$  is the baryon mass fraction taken into the disk. Substituting Equations (26), (27), (28), and (29) into the above, we obtain number density at the center of the disk

$$n_0 = 2.0 \times 10^4 \text{cm}^{-3} \left( \frac{f_d}{0.5} \right)^2 \left( \frac{\lambda}{0.05} \right)^{-4} \left( \frac{1+z_{\text{vir}}}{10} \right)^4 \times \left( \frac{T}{8000 \text{K}} \right)^{-1} \left( \frac{M_h}{10^9 M_\odot} \right)^{2/3}. \quad (31)$$

From Equation (29), the scale height of the disk is

$$z_0 = 1.6 \text{pc} \left( \frac{f_d}{0.5} \right)^{-1} \left( \frac{\lambda}{0.05} \right)^2 \left( \frac{1+z_{\text{vir}}}{10} \right)^{-2} \times \left( \frac{T}{8000 \text{K}} \right) \left( \frac{M_h}{10^9 M_\odot} \right)^{-1/3} \exp\left(\frac{r}{R_d}\right), \quad (32)$$

and the disk surface density is

$$\begin{aligned} \Sigma_{\text{gas}}(r) &= \int dz \mu m_H n(r, z) \\ &= 0.46 \text{g cm}^{-2} \left( \frac{f_d}{0.5} \right) \left( \frac{\lambda}{0.05} \right)^{-2} \left( \frac{1+z_{\text{vir}}}{10} \right)^2 \\ &\quad \times \left( \frac{M_h}{10^9 M_\odot} \right)^{1/3} \exp\left(-\frac{r}{R_d}\right). \end{aligned} \quad (33)$$

As in Section 2.1, we estimate the SFE  $\epsilon_*$  by Equation

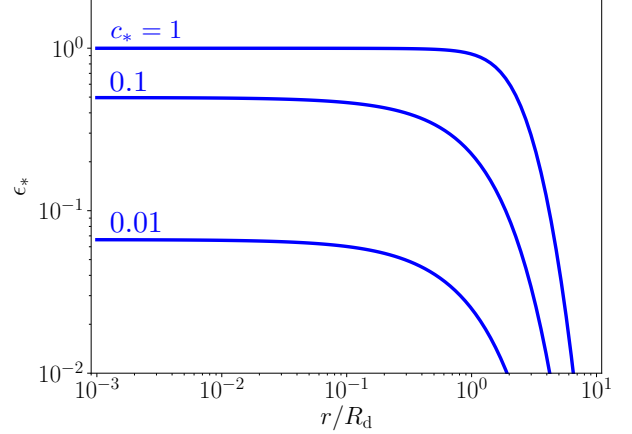


**Figure 8.** The radial distribution of SFE in a galactic disk with  $M_h = 10^9 M_\odot$ ,  $1+z_{\text{vir}} = 10$ ,  $T_g = 8000 \text{K}$ ,  $f_d = 0.5$  and  $\lambda = 0.05$  for three values of the star-formation rate parameter  $c_* = 1, 0.1$ , and  $0.01$  from top to bottom.

(7). Since the gas density does not decrease remarkably up to the scale height  $z_0$  according to Equation (28), we use the density on the equatorial plane ( $z = 0$ ) in calculating  $\epsilon_*$  in the disk. The radial distribution of SFE is presented in Figure 8 for three cases of  $c_* = 1, 0.1$ , and  $0.01$ . The SFE is almost constant inside the disk radius  $R_d$  and decreases rapidly outside. In the case with  $c_* = 1$ , the SFE is as high as  $\sim 1$  in the disk. The stellar surface density is thus given by

$$\begin{aligned} \Sigma_* &= \epsilon_* \Sigma_{\text{gas}} \\ &= 2.2 \times 10^2 M_\odot \text{pc}^{-2} \left( \frac{f_d}{0.5} \right) \left( \frac{\lambda}{0.05} \right)^{-2} \\ &\quad \times \left( \frac{1+z_{\text{vir}}}{10} \right)^2 \left( \frac{\epsilon_*}{0.1} \right) \left( \frac{M_h}{10^9 M_\odot} \right)^{1/3} \exp\left(-\frac{r}{R_d}\right). \end{aligned} \quad (34)$$

The luminosity and the ionizing photon emissivity per unit area,  $\mathcal{L}$  and  $\mathcal{S}$ , can be calculated from the surface density of stars  $\Sigma_*$  and luminosity/emissivity per unit stellar mass given in Table 1. For example, in the case of  $m_{\text{ch}} = 10 M_\odot$ , they are

$$\begin{aligned} \mathcal{L} &= 1.5 \times 10^6 L_\odot \text{pc}^{-2} \left( \frac{f_d}{0.5} \right) \left( \frac{\lambda}{0.05} \right)^{-2} \left( \frac{1+z_{\text{vir}}}{10} \right)^2 \\ &\quad \times \left( \frac{\epsilon_*}{0.1} \right) \left( \frac{M_h}{10^9 M_\odot} \right)^{1/3} \exp\left(-\frac{r}{R_d}\right), \end{aligned} \quad (35)$$

and

$$\begin{aligned} \mathcal{S} &= 1.1 \times 10^{50} \text{s}^{-1} \text{pc}^{-2} \left( \frac{f_d}{0.5} \right) \left( \frac{\lambda}{0.05} \right)^{-2} \left( \frac{1+z_{\text{vir}}}{10} \right)^2 \\ &\quad \times \left( \frac{\epsilon_*}{0.1} \right) \left( \frac{M_h}{10^9 M_\odot} \right)^{1/3} \exp\left(-\frac{r}{R_d}\right). \end{aligned} \quad (36)$$

#### 3.2 Dust evacuation time from galactic disks

We assume that stars are distributed on the mid-plane of galactic disks. As in Section 2.2, we derive the condition for dust evacuation by calculating the evacuation time  $t_{\text{evac}}$  at the scale height  $z = z_0$  (Eq. 29). We use the cylindrical

coordinate  $(r, \theta, z)$  where the  $z$ -axis passes through the center of the galaxy and perpendicular to the disks. From the axisymmetry, no  $\theta$ -dependence appears.

Using the SFE  $\epsilon_*$  (Eq. 7), the luminosity and the ionizing photon emissivity per unit area in the disk are given as (Eqs. 35 and 36),

$$\mathcal{L} = \mathcal{L}_0 \left( 1 - \exp \left[ -c_* \frac{t_{\text{OB}}}{t_{\text{ff}}} \exp(-r/R_d) \right] \right) \exp(-r/R_d), \quad (37)$$

and

$$\mathcal{S} = \mathcal{S}_0 \left( 1 - \exp \left[ -c_* \frac{t_{\text{OB}}}{t_{\text{ff}}} \exp(-r/R_d) \right] \right) \exp(-r/R_d), \quad (38)$$

where

$$\mathcal{L}_0 = 1.5 \times 10^7 L_\odot \text{pc}^{-2} \left( \frac{f_d}{0.5} \right) \left( \frac{\lambda}{0.05} \right)^{-2} \left( \frac{1+z_{\text{vir}}}{10} \right)^2 \left( \frac{M_h}{10^9 M_\odot} \right)^{1/3}, \quad (39)$$

and

$$\mathcal{S}_0 = 1.1 \times 10^{51} \text{s}^{-1} \text{pc}^{-2} \left( \frac{f_d}{0.5} \right) \left( \frac{\lambda}{0.05} \right)^{-2} \left( \frac{1+z_{\text{vir}}}{10} \right)^2 \left( \frac{M_h}{10^9 M_\odot} \right)^{1/3}. \quad (40)$$

The  $r$ - and  $z$ -components of the radiation force on a dust grain with radius  $a$  locating at  $(r_0, z_0)$  are

$$\begin{aligned} F_{\text{rad},r} &= \frac{\pi a^2 Q}{4\pi c} \int_0^\infty dr \int_0^{2\pi} r d\theta \frac{-(r \cos \theta - r_0)}{[r^2 + r_0^2 - 2rr_0 \cos \theta + z_0^2]^{3/2}} \mathcal{L} \\ &= \frac{\pi a^2 Q \mathcal{L}_0}{4\pi c} \phi_r, \end{aligned} \quad (41)$$

and

$$\begin{aligned} F_{\text{rad},z} &= \frac{\pi a^2 Q}{4\pi c} \int_0^\infty dr \int_0^{2\pi} r d\theta \frac{z_0}{[r^2 + r_0^2 - 2rr_0 \cos \theta + z_0^2]^{3/2}} \mathcal{L} \\ &= \frac{\pi a^2 Q \mathcal{L}_0}{4\pi c} \phi_z, \end{aligned} \quad (42)$$

respectively. With definition of  $\mathcal{R} = r/R_d$ ,  $\mathcal{R}_0 = r_0/R_d$ ,  $\mathcal{Z}_0 = z_0/R_d$  and  $C = c_* t_{\text{OB}}/t_{\text{ff}}$ ,

$$\begin{aligned} \phi_r &= \int_0^\infty d\mathcal{R} \int_0^{2\pi} d\theta \frac{(\mathcal{R}_0 - \mathcal{R} \cos \theta) \mathcal{R}}{[(\mathcal{R}^2 + \mathcal{R}_0^2 - 2\mathcal{R}\mathcal{R}_0 \cos \theta) + \mathcal{Z}_0^2]^{3/2}} \\ &\quad \times (1 - \exp[-C \exp(-\mathcal{R})]) \exp(-\mathcal{R}), \end{aligned} \quad (43)$$

and

$$\begin{aligned} \phi_z &= \int_0^\infty d\mathcal{R} \int_0^{2\pi} d\theta \frac{\mathcal{R} \mathcal{Z}_0}{[(\mathcal{R}^2 + \mathcal{R}_0^2 - 2\mathcal{R}\mathcal{R}_0 \cos \theta) + \mathcal{Z}_0^2]^{3/2}} \\ &\quad \times (1 - \exp[-C \exp(-\mathcal{R})]) \exp(-\mathcal{R}). \end{aligned} \quad (44)$$

The radial dependence of  $\phi_r$  and  $\phi_z$  is presented in Figure 9.

The dust terminal velocity is estimated by the balance between the radiation force  $F_{\text{rad}} = \sqrt{(F_{\text{rad},r})^2 + (F_{\text{rad},z})^2}$  and the collisional drag force  $F_{\text{drag}} = \pi a^2 v_d^2 n_{\text{H}} m_{\text{H}}$ . Here, we consider the dust evacuation in the vertical direction. The vertical component of terminal velocity  $v_{d,z}$  is

$$v_{d,z} = \sqrt{\frac{\mathcal{L}_0 Q}{4\pi c n_{\text{H}} m_{\text{H}}}} \phi_z (\phi_r^2 + \phi_z^2)^{-1/4}, \quad (45)$$

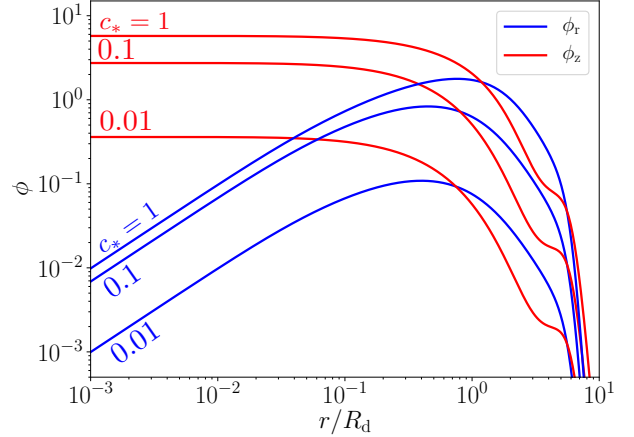


**Figure 9.** The radial dependence of  $\phi_r$  (blue) and  $\phi_z$  (red) in the case with  $\mathcal{Z}_0 = 2.0 \times 10^{-2} \exp(\mathcal{R}_0)$ . The different lines show the cases with  $c_* = 1, 0.1, \text{ and } 0.01$  from top to bottom.

whose value at the center of the disk is

$$\begin{aligned} v_{d,z}(r=0) &= 1.4 \times 10^6 \text{cm s}^{-1} \left( \frac{f_d}{0.5} \right)^{-1/2} \left( \frac{\lambda}{0.05} \right) \left( \frac{1+z_{\text{vir}}}{10} \right)^{-1} \\ &\quad \times \left( \frac{\phi_z}{2.7} \right)^{1/2} \left( \frac{T_{\text{gas}}}{8000 \text{K}} \right)^{1/2} \left( \frac{Q}{1} \right)^{1/2} \left( \frac{M_h}{10^9 M_\odot} \right)^{-1/6}. \end{aligned} \quad (46)$$

Figure 10 shows the radial dependence of the dust terminal velocity  $v_{d,z}$  (Eq. 45) at a disk scale height ( $z = z_0$ ). The terminal velocity is almost constant inside the disk radius  $R_d$ , and increases outward as the drag force becomes small with decreasing gas density.

The dust evacuation time  $t_{\text{evac}}$  is given by

$$\begin{aligned} t_{\text{evac}} &= \frac{z_0}{v_{d,z}} \\ &= 1.1 \times 10^5 \text{yr} \left( \frac{f_d}{0.5} \right)^{-1/2} \left( \frac{\lambda}{0.05} \right) \left( \frac{1+z_{\text{vir}}}{10} \right)^{-1} \left( \frac{\phi_z}{2.7} \right)^{-1/2} \\ &\quad \times \left( \frac{T_{\text{gas}}}{8000 \text{K}} \right)^{1/2} \left( \frac{Q}{1} \right)^{-1/2} \left( \frac{M_h}{10^9 M_\odot} \right)^{-1/6}. \end{aligned} \quad (47)$$

In Figure 11, we show the radial dependence of dust evacuation time  $t_{\text{evac}}$ . It is almost constant inside the disk radius  $R_d$  as expected from the behavior of  $v_{d,z}$  and increases rapidly at  $r > R_d$  due to the increasing scale height (Eq. 32).

### 3.3 Vertical expansion of the HII region in the disk

We seek the condition for star formation from dust-free galactic disks by comparing the lifetime of OB stars,  $t_{\text{OB}}$ , and the expansion time of the HII region,  $t_{\text{HII}}$ , with the dust evacuation time,  $t_{\text{evac}}$ , as in Section 2.3 and 2.4.

We define the Strömgen height  $z_{\text{S0}}$  where the number of ionizing photons emitted from  $z = 0$  equals the integrated recombination rate of hydrogen atoms:

$$\int_{-z_{\text{S0}}}^{z_{\text{S0}}} dz n_{\text{H}}^2 \alpha_{\text{B}} = \mathcal{S}. \quad (48)$$

The ionizing-photon emissivity per unit area  $\mathcal{S}$  is given by



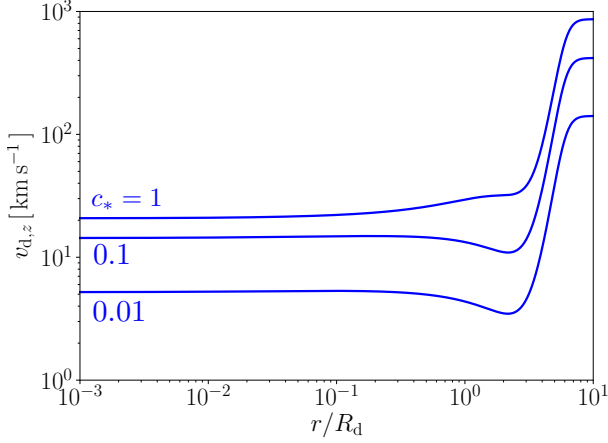


**Figure 10.** The vertical component of the dust velocity  $v_{d,z}$  at the scale height  $z_0$  as a function of radius  $r$  in the case with  $f_d = 0.5$ ,  $\lambda = 0.05$ ,  $1 + z_{\text{vir}} = 10$ ,  $T_{\text{gas}} = 8000$  K,  $Q = 1$ ,  $\epsilon_* = 0.1$  and  $M_h = 10^9 M_\odot$ . The different lines show the case with  $c_* = 1$ , 0.1 and 0.01, from the top to the bottom.

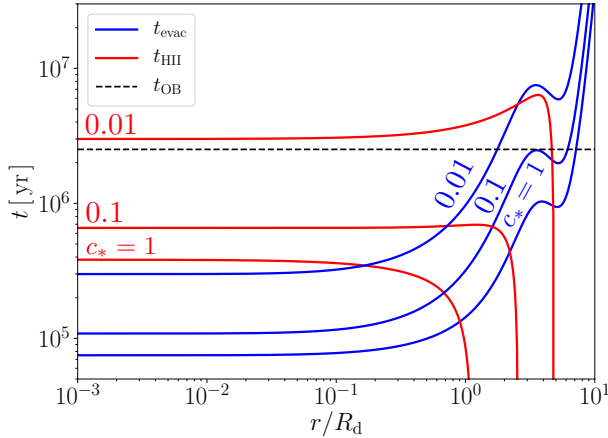


**Figure 11.** Dust evacuation time  $t_{\text{evac}}$ , expansion time of HII regions  $t_{\text{HII}}$  and lifetime of OB stars  $t_{\text{OB}}$  at the disk scale height  $z_0$  in the case with  $f_d = 0.5$ ,  $\lambda = 0.05$ ,  $1 + z_{\text{vir}} = 10$ ,  $T = 8000$  K,  $Q = 1$ ,  $\epsilon_* = 0.1$  and  $M_h = 10^9 M_\odot$ . The cases with  $c_* = 1$ , 0.1, and 0.01 are shown as indicated for  $t_{\text{evac}}$  and  $t_{\text{HII}}$ .

Equation (39). Neglecting the density variation with height and substituting Equation (28), (31) and (39) into (48), we obtain

$$z_{\text{S0}} = 1.9 \times 10^{-2} \text{ pc} \left( \frac{f_d}{0.5} \right)^{-3} \left( \frac{\lambda}{0.05} \right)^6 \left( \frac{1 + z_{\text{vir}}}{10} \right)^{-6} \times \left( \frac{T}{8000 \text{ K}} \right)^2 \left( \frac{\epsilon_*}{0.1} \right) \left( \frac{M_h}{10^9 M_\odot} \right)^{-1} \exp \left( \frac{3r}{R_d} \right). \quad (49)$$

As in Equation (24), the time for the HII region to expand up to  $z = z_0$  is estimated as

$$t_{\text{HII}} = \frac{4}{7} \frac{z_{\text{S0}}}{c_{\text{HII}}} \left[ \left( \frac{z_0}{z_{\text{S0}}} \right)^{7/4} - 1 \right]. \quad (50)$$

In particular, at the center of the disk,

$$t_{\text{HII}}(r = 0) = 2.2 \times 10^6 \text{ yr} \left( \frac{f_d}{0.5} \right)^{1/2} \left( \frac{\lambda}{0.05} \right)^{-1} \left( \frac{1 + z_{\text{vir}}}{10} \right) \times \left( \frac{T}{8000 \text{ K}} \right)^{1/4} \left( \frac{\epsilon_*}{0.1} \right)^{-3/4} \left( \frac{M_h}{10^9 M_\odot} \right)^{1/6}. \quad (51)$$

The expansion time of the HII region  $t_{\text{HII}}$  is shown in Figure 11 as a function of the radius. At  $r < R_d$ ,  $t_{\text{HII}}$  is longer than  $t_{\text{evac}}$  because the initial Strömgen height of the HII region  $z_{\text{S0}}$  (Eq. 49) is much smaller than the disk scale height  $z_0$ . As the radius exceeds  $R_d$ , the scale height of the HII region  $z_{\text{HII}}$  rapidly increases, resulting in shorter  $t_{\text{HII}}$  than  $t_{\text{evac}}$ .

### 3.4 Condition for dust evacuation from galactic disks

For the dust evacuation (Eq. 21), the evacuation time  $t_{\text{evac}}$  must be shorter than lifetime of the cloud,  $t_{\text{cl}} = \min(t_{\text{OB}}, t_{\text{HII}})$ . For example, in Figure 11 for the halo shown ( $M_h = 10^9 M_\odot$ ,  $1 + z_{\text{vir}} = 10$ ,  $T_{\text{gas}} = 8000$  K,  $\lambda = 0.05$  and  $f_d = 0.5$ ), the dust evacuation occurs inside the galactic disk  $r < R_d$  and the dust-free gas is formed in all the three cases.

Additionally, there is a condition on metallicity of the gas. As explained in Section 2.2, the direct light from stars is absorbed and re-emitted as thermal emission of dust grains in optically thick disks, and radiation force on dust grains becomes about two orders of magnitude smaller. Therefore, the optical depth to the direct light along the vertical direction must be less than unity for the dust evacuation:

$$\tau = \int_{-\infty}^{\infty} \rho k dz = 1.6 \times 10^2 \left( \frac{Z}{Z_\odot} \right) \left( \frac{f_d}{0.5} \right) \left( \frac{\lambda}{0.05} \right)^{-2} \left( \frac{1 + z_{\text{vir}}}{10} \right)^2 \times \left( \frac{\kappa}{350 \text{ cm}^2 \text{ g}^{-1}} \right) \left( \frac{M_h}{10^9 M_\odot} \right)^{1/3} \exp \left( \frac{-2r}{R_d} \right) < 1. \quad (52)$$

This requires low metallicity environments of

$$Z < 6.1 \times 10^{-3} Z_\odot \left( \frac{f_d}{0.5} \right)^{-1} \left( \frac{\lambda}{0.05} \right)^2 \left( \frac{1 + z_{\text{vir}}}{10} \right)^{-2} \times \left( \frac{\kappa}{350 \text{ cm}^2 \text{ g}^{-1}} \right)^{-1} \left( \frac{M_h}{10^9 M_\odot} \right)^{-1/3}. \quad (53)$$

Next we derive the constraint on the halo mass  $M_h$  and redshift  $1 + z_{\text{vir}}$  under the condition of the spin parameter  $\lambda = 0.05$  and the baryon mass fraction taken into the disks  $f_d = 0.5$ . Figure 12 shows the range of halo parameters for the dust evacuation from the disks. Note that since the timescale  $t_{\text{evac}}$  and  $t_{\text{cl}}$  hardly change inside the disk  $r < R_d$ , it suffices to consider the condition  $t_{\text{evac}} < t_{\text{cl}}$  at the center ( $r = 0$ ). In Figure 12, black, red and blue colors correspond to the cases with the SFR parameter  $c_* = 1$ , 0.1, and 0.01, respectively. The condition  $t_{\text{evac}} < t_{\text{cl}}$  is satisfied above the solid line, but above the dashed line the SFE is already  $> 0.9$  at  $t_{\text{evac}}$ . Thus, the color-shaded regions between the two lines represents the parameter space where the dust evacuation occurs and gases still remain at this time, resulting in star formation from the dust-free gas. Also the thin-dotted lines

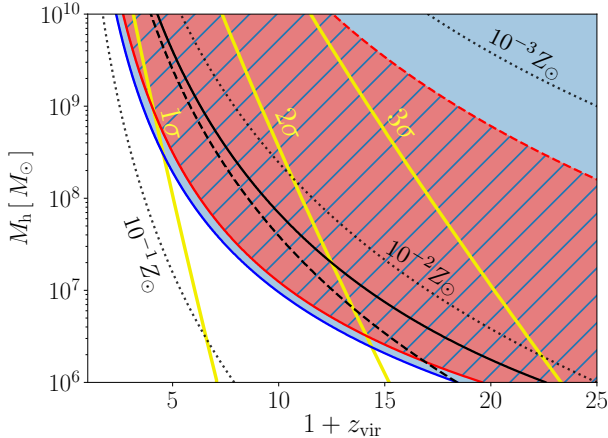


**Figure 12.** Conditions for the dust evacuation from galactic disks. The thick solid lines correspond to the halo mass  $M_h$  satisfying the condition  $t_{\text{evac}} = t_{\text{cl}}$ . The thick dashed lines show the galaxies where the SFE becomes  $\epsilon_* = 0.9$ . Black, red and blue colors correspond to the cases with  $c_* = 1, 0.1$  and  $0.01$ , respectively. The color-shaded areas between them represent the regions that satisfy both the conditions  $t_{\text{evac}} < t_{\text{cl}}$  and  $\epsilon_* < 0.9$ . Namely, those conditions are satisfied in the upper side of the blue-solid line (both in the blue and red shaded regions) for  $c_* = 0.1$ , and between the red-solid and red-dashed lines (in the red-shaded region) for  $c_* = 0.01$ , respectively. In the case with  $c_* = 1$ , there is no such region. The galactic disks become optically thin below the thin dotted lines for the indicated metallicity. The yellow-solid lines show the halo mass and redshift when  $1, 2$  and  $3\sigma$  fluctuations are virialized (Barkana & Loeb 2001; Eisenstein & Hu 1998, 1999; Planck Collaboration 2016).

show the contour of the maximum metallicity allowed (Eq. 53) for a dust evacuation for a given parameter set ( $M_h, z_{\text{vir}}$ ). Additionally, the yellow-solid lines show the relation between the halo mass and the formation redshift for the  $1, 2$  and  $3\sigma$  cosmological density fluctuations. Here, we use the cosmological parameters of Planck Collaboration (2016) and Eisenstein & Hu (1998, 1999).

For higher halo mass and formation redshift, the dust evacuation time  $t_{\text{evac}}$  is shorter (Eq. 47) and the HII region expansion time  $t_{\text{HII}}$  is longer (Eq. 51). Thus the minimum halo mass for the dust evacuation increases with decreasing redshift. As an example, for a halo with mass  $M_h = 10^9 M_\odot$ , the condition for dust evacuation is satisfied if formed at  $z_{\text{vir}} \gtrsim 3$  with metallicity  $Z \lesssim 10^{-1} - 10^{-2} Z_\odot$  with little dependence on  $c_*$ . With lower halo mass, formation redshift must be earlier, e.g.,  $z_{\text{vir}} \gtrsim 9$  with  $M_h = 10^7 M_\odot$ . As shown in Figure 12, the lowest halo mass for the dust evacuation is equivalent to the  $2\sigma$  ( $1\sigma$ ) fluctuation at  $z_{\text{vir}} \approx 15$  ( $\approx 5$ , respectively). With larger value of  $c_*$ , the HII region expansion time,  $t_{\text{HII}}$ , becomes shorter. In addition, since the galactic disk must be optically thin, the dust evacuation only occurs at metallicity lower than  $\sim 10^{-2} Z_\odot$ , depending somewhat on the halo mass and formation redshift.

## 4 CAVEATS

In Sections 2 and 3, we have modelled the dust evacuation under the assumption that the ionization degree is

lower than  $\sim 10^{-5}$  so that the Coulomb drag is inefficient. The cosmic rays (CRs) or X-rays from nearby star-forming galaxies, however, can boost the ionization degree in the interstellar medium. In addition, although we assumed the efficiency factor of dust photo-absorption  $Q = 1$  in calculating the evacuation time, it becomes smaller for grains with size  $\lesssim 0.01 \mu\text{m}$  and the radiation force on dust becomes weaker. Also, we have not considered magnetic fields, which prevents the perpendicular motion of charged grains. In the following, we discuss those effects on the dust evacuation.

### 4.1 Possible enhancement of ionization degree

As discussed in Section 2.2, the Coulomb drag suppresses the motion of dust grains and makes the evacuation time longer than the lifetime of massive stars for ionization degree  $x_e > 10^{-5}$ . The increase of ionization degree is likely caused by the cosmic rays, X-rays from nearby galaxies, or mixing with ionized gas from HII regions or stellar winds. In the following, we estimate their impact on the ionization degree.

#### 4.1.1 Cosmic rays

We here follow Stacy & Bromm (2007) for estimating the ionization degree by CRs, which were supposed to be produced in SN remnants in a different nearby galaxy. Since we are considering the dust evacuation before the first SN explodes, we assume the CRs and X-rays are coming from other nearby galaxies. The ionization rate  $\xi_{\text{CR}}$  is related with the energy density of CRs  $U_{\text{CR}}$  as:

$$\xi_{\text{CR}} = 1.4 \times 10^{-17} \text{s}^{-1} \left( \frac{U_{\text{CR}}}{10^{-15} \text{erg cm}^{-3}} \right), \quad (54)$$

where the energy distribution is assumed to be the same power law as in the Milky Way with the slope  $-2.65$  (Blümer et al. 2009; Draine 2011b), ranging from  $10^6 \text{eV}$  to  $10^{15} \text{eV}$ . Assuming an efficiency  $0.1$  of SN energy  $10^{51} \text{erg}$  is used in the CR acceleration, we adopt the total CR energy generated in a SN remnant  $E_{\text{CR}} = 10^{50} \text{erg}$ . Using the mass fraction of massive stars  $f_{\text{OB}} = 0.74$  and their average mass  $\bar{m}_{\text{OB}} = 29 M_\odot$  for the IMF of Equation (8), the SN rate is

$$\begin{aligned} \dot{N}_{\text{SN}} &= \frac{f_{\text{OB}} \text{SFR}}{\bar{m}_{\text{OB}}} \\ &= 2.6 \times 10^{-2} \text{yr}^{-1} \left( \frac{\text{SFR}}{1 M_\odot \text{yr}^{-1}} \right). \end{aligned} \quad (55)$$

At the distance  $d$  from the CR source galaxy, the CR energy density is given by

$$\begin{aligned} U_{\text{CR}} &= \frac{\dot{N}_{\text{SN}} E_{\text{CR}}}{4\pi d^2 v_{\text{CR}}} \\ &= 3.4 \times 10^{-15} \text{erg cm}^{-3} \left( \frac{d}{10 \text{kpc}} \right)^{-2} \left( \frac{\text{SFR}}{1 M_\odot \text{yr}^{-1}} \right), \end{aligned} \quad (56)$$

where  $v_{\text{CR}} = 8.8 \times 10^{-2} c$  is the average velocity of CRs (Stacy & Bromm 2007). By substituting Equation (56) into Equation (54), we obtain the CR ionization rate:

$$\xi_{\text{CR}} = 4.8 \times 10^{-17} \text{s}^{-1} \left( \frac{d}{10 \text{kpc}} \right)^{-2} \left( \frac{\text{SFR}}{1 M_\odot \text{yr}^{-1}} \right). \quad (57)$$

Using this rate in Equation (15), the ionization degree is given by

$$x_e = 3.5 \times 10^{-5} \left( \frac{R_{\text{cl}}}{10 \text{ pc}} \right)^{3/2} \times \left( \frac{M_{\text{cl}}}{10^6 M_\odot} \right)^{-1/2} \left( \frac{d}{10 \text{ kpc}} \right)^{-1} \left( \frac{\text{SFR}}{1 M_\odot \text{ yr}^{-1}} \right)^{1/2}. \quad (58)$$

This means that if the source galaxy with  $\text{SFR} \gtrsim 1 M_\odot \text{ yr}^{-1}$  is within 40 kpc, the CRs raise the ionization degree above the threshold value  $10^{-5}$  for the Coulomb drag, resulting in the suppression of the dust evacuation.

In the above discussion, we assumed that CRs stream away freely from the source galaxy. Magnetic fields, if present with sufficient strength, confine CRs in the source galaxy. Given that SN remnants are inside the galaxy, the CR intensity is enhanced not only by their proximity but also by this magnetic effect. In this case, the ionization degree becomes much higher compared with Equation (58), and the dust evacuation is strongly inhibited. In contrast, if the CR sources are outside the galaxy under consideration, the ionization rate would be reduced because the magnetic field protects the galaxy from the CR incidence.

#### 4.1.2 X-rays

Massive binary stars can evolve to X-ray binaries. We evaluate the ionization by such X-ray sources based on the model of Glover & Brand (2003). We again assume the sources are in a nearby galaxy at distance  $d$  from the cloud under consideration. The X-ray luminosity is related to the star formation rate as

$$L_X = 6.0 \times 10^{38} \text{ erg s}^{-1} \left( \frac{\text{SFR}}{1 M_\odot \text{ yr}^{-1}} \right). \quad (59)$$

For the power-law spectrum with the slope  $-1.5$ , the X-ray intensity is given by

$$J_X = 2.3 \times 10^{-25} \text{ erg s}^{-1} \text{ cm}^{-2} \text{ sr}^{-1} \text{ Hz}^{-1} \times \left( \frac{\nu}{\nu_0} \right)^{-1.5} \left( \frac{d}{10 \text{ kpc}} \right)^{-2} \left( \frac{\text{SFR}}{1 M_\odot \text{ yr}^{-1}} \right), \quad (60)$$

where  $h\nu_0 = 1 \text{ eV}$ . The primary ionization rate of X-rays is thus given by

$$\xi_{X,p} = \int \frac{4\pi J_X(\nu)}{h\nu} \sigma_H(\nu) d\nu = 6.8 \times 10^{-23} \text{ s}^{-1} \left( \frac{d}{10 \text{ kpc}} \right)^{-2} \left( \frac{\text{SFR}}{1 M_\odot \text{ yr}^{-1}} \right), \quad (61)$$

where  $\sigma_H(\nu)$  is the cross section of hydrogen and we have set the energy range from 2 keV to 10 keV. Secondary ionization is dominant in the case of X-ray ionization. Using the secondary ionization rate  $\phi^H$  by Wolfire et al. (1995), we obtain the X-ray ionization rate as

$$\xi_X = \xi_{X,p}(1 + \phi^H) = 8.8 \times 10^{-21} \text{ s}^{-1} \left( \frac{d}{10 \text{ kpc}} \right)^{-2} \left( \frac{\text{SFR}}{1 M_\odot \text{ yr}^{-1}} \right). \quad (62)$$

Comparing with the CR ionization (Eq. 57), X-ray ionization rate is more than two orders of magnitude lower and has little impact on the dust evacuation.

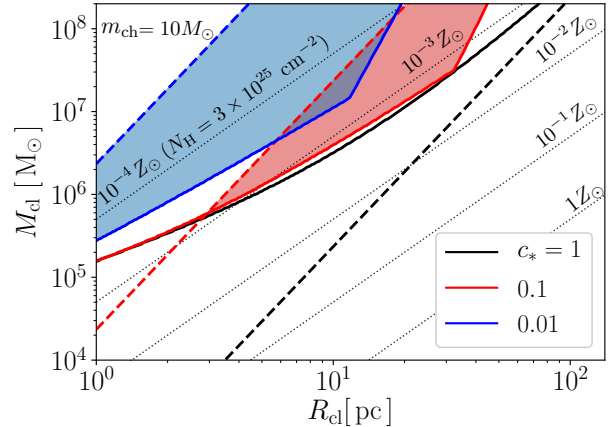


**Figure 13.** Same as Figure 5, but for the case of the smaller efficiency factor of  $Q = 0.3$ .

#### 4.1.3 Mixing with ionized medium

Near the boundary with ionized gases such as the HII regions or ionized stellar winds, mixing with neutral and ionized medium may occur due, e.g., to hydrodynamical instabilities. Although this raises the ionization degree in the neutral gas temporarily, it decreases in the recombination time, which can be estimated for the ionization degree  $x_e = 10^{-5}$  as

$$t_{\text{rec}} = (\alpha_B n_H x_e)^{-1} = 4.5 \times 10^4 \text{ yr} \left( \frac{n_H}{10^4 \text{ cm}^{-3}} \right)^{-1} \left( \frac{x_e}{10^{-5}} \right)^{-1}. \quad (63)$$

Since the recombination time is much shorter than the dust evacuation time  $t_{\text{evac}}$  (Eq. 17, 47), mixing with the ionized gas does not affect the dust evacuation unless the ionized gas is constantly supplied by some mechanism in a timescale shorter than  $\sim t_{\text{rec}}$ .

## 4.2 Small dust grains

In previous sections, we assumed that the dust absorption efficiency factor  $Q = 1$ , corresponding to grains larger than  $\sim 0.01 \mu\text{m}$ . If small grains are dominant, however, the efficiency factor decreases and the dust evacuation time becomes longer as  $Q^{-1/2}$  (Eqs. 17 and 47).

Dust grains in the early Universe (at  $z > 6$ ) are mainly produced in SN events because intermediate-mass stars ( $< 8 M_\odot$ ) take more than 1 Gyr to become AGB stars which produce a large quantity of dust grains (Morgan & Edmunds 2003; Dwek et al. 2007). Theoretical calculations indicate that small grains  $a < 0.01 \mu\text{m}$  have a flat “top-heavy” size distribution in the early Universe (Todini & Ferrara 2001; Schneider et al. 2012), unlike the so-called MRN distribution (Mathis et al. 1977) in the local interstellar medium, which has a “bottom-heavy” power-law with the slope  $\alpha = -3.5$  in the range  $a \sim 0.01 - 1.0 \mu\text{m}$ . In addition, small grains  $\lesssim 0.05 \mu\text{m}$  are subsequently destroyed by the passage of the SN reverse shock in their formation site (Nozawa et al. 2007; Bianchi & Schneider 2007). Since the efficiency factor  $Q \sim 1$  (Figure 3) for grains larger than  $0.01 \mu\text{m}$ , our

assumption  $Q = 1$  would be reasonable for dust in the early universe. Considering uncertainties in the dust size distribution, however, we also calculate the case of small grains with  $a = 5 \times 10^{-3} \mu\text{m}$ , which have  $Q \simeq 0.3$ . Figure 13 presents the condition for formation of dust-free star-forming clouds. Due to smaller efficiency factor, the parameter range for the dust-free cloud formation becomes smaller compared to the fiducial case (Figure 5). Only massive compact clouds satisfy the dust evacuation condition if the typical dust size is smaller than  $\sim 0.01 \mu\text{m}$ . Further studies are needed about the size distribution of grains in the early Universe.

### 4.3 Magnetic field

Dust grains have positive electric charge due to photoelectric effect so that their motion is influenced by the presence of magnetic field. In fact, the gyro-radius of a grain

$$\begin{aligned} r_{\text{gyro}} &= \frac{m_d v_d c}{qB} \\ &= 9.4 \times 10^{-7} \text{ pc} \left( \frac{q}{600 e} \right)^{-1} \left( \frac{B}{100 \mu\text{G}} \right)^{-1} \\ &\quad \times \left( \frac{\rho_d}{3 \text{ g cm}^{-3}} \right) \left( \frac{a_d}{0.1 \mu\text{m}} \right)^3 \left( \frac{v_d}{7 \text{ km s}^{-1}} \right), \end{aligned} \quad (64)$$

is much smaller than the star-forming regions if the magnetic field is as strong as in local molecular clouds  $\sim 100 \mu\text{G}$  (Crutcher 1999).

Below, we evaluate the dust drift velocity taking the effect of magnetic field into account (Draine 2011a). For simplicity, we assume that the magnetic field is parallel to the  $z$ -axis,  $\mathbf{B} = (0, 0, B)$ , and the radiation force direction is at angle  $\theta$  to the field orientation,  $\mathbf{F}_{\text{rad}} = (F_{\text{rad}} \sin \theta, 0, F_{\text{rad}} \cos \theta)$ . Dust grains have steady time-averaged velocity  $\bar{\mathbf{v}}$  with rotational motion around the magnetic field, with  $x$ ,  $y$ , and  $z$ -components, respectively,

$$\bar{v}_x = \frac{1}{1 + (\omega t_{\text{drag}})^2} \frac{F_{\text{rad}} t_{\text{drag}}}{m_d} \sin \theta, \quad (65)$$

$$\bar{v}_y = -\frac{(\omega t_{\text{drag}})}{1 + (\omega t_{\text{drag}})^2} \frac{F_{\text{rad}} t_{\text{drag}}}{m_d} \sin \theta, \quad (66)$$

$$\bar{v}_z = \frac{F_{\text{rad}} t_{\text{drag}}}{m_d} \cos \theta. \quad (67)$$

The drift velocity becomes

$$v_d = \sqrt{\frac{1 + \cos^2 \theta (\omega t_{\text{drag}})^2}{1 + (\omega t_{\text{drag}})^2}} \frac{F_{\text{rad}} t_{\text{drag}}}{m_d}, \quad (68)$$

where  $\omega = qB/m_d c$  is the gyro-frequency and  $t_{\text{drag}}$  is the drag time (Eq. 18). From Equation (68), we can see that the magnetic field greatly hinders the grain motion when

$$\begin{aligned} \omega t_{\text{drag}} &= 0.26 \left( \frac{q}{600 e} \right) \left( \frac{B}{0.1 \mu\text{G}} \right) \left( \frac{a_d}{0.1 \mu\text{m}} \right)^{-2} \\ &\quad \times \left( \frac{v_d}{7 \text{ km s}^{-1}} \right)^{-1} \left( \frac{n_{\text{H}}}{10^4 \text{ cm}^{-3}} \right)^{-1} \end{aligned} \quad (69)$$

is much larger than unity. In particular, the dust velocity is reduced by a factor of  $1/\sqrt{1 + (\omega t_{\text{drag}})^2}$  from the value without a magnetic field when the direction of the radiation force

is vertical to the field. Magnetic fields in first galaxies are usually expected to be much weaker than in the Milky Way (Koh & Wise 2016). As seen in Equation (69), as long as the field is weaker than  $\sim 0.1 \mu\text{G}$ ,  $\omega t_{\text{drag}} \leq 1$  and the dust evacuation is not suppressed. Magnetic fields, however, can be potentially amplified by turbulent small-scale dynamo to equipartition, which corresponds to  $\sim 100 \mu\text{G}$  (Schober et al. 2012). In this case, the dust drift in the vertical direction is strongly suppressed but dust grains can still drift in the direction along magnetic fields. Thus, the suppression effect by magnetic fields would remain at the factor of a few level. For further discussion on this problem, detailed numerical calculation is awaited.

## 5 SUMMARY AND DISCUSSION

We have investigated whether the dust grains are evacuated from star-forming regions by stellar radiation feedback so that star formation from the dust-free gas ensues in some environments in the early universe. We have obtained the condition for the dust evacuation by comparing the dust evacuation time,  $t_{\text{evac}}$ , with the smaller of the HII region expansion time,  $t_{\text{HII}}$ , and the OB star lifetime  $t_{\text{OB}}$ .

Our findings are summarized as follows:

- (1) As star-forming clouds become compact, the evacuation time decreases. Therefore, the dust evacuation can occur for compact star-forming clouds whose column density is  $N_{\text{H}} \simeq 10^{24} \sim 10^{26} \text{ cm}^{-2}$ , corresponding to the radius of 1–10 pc for the mass  $M_{\text{cl}} = 10^6 M_{\odot}$ . The radiation force on dust grains is reduced significantly if the clouds are optically thick to the radiation from stars. This imposes the condition that metallicity should be less than  $\sim 10^{-2} Z_{\odot}$ .
- (2) The dust evacuation from galactic disks occurs more easily in more massive halos and at earlier formation redshift. For example, halos of  $\sim 10^9 M_{\odot}$  ( $\sim 10^7 M_{\odot}$ ) formed at  $z \sim 3$  ( $z \sim 9$ , respectively) can induce the dust evacuation. We find that  $t_{\text{evac}}$  and  $t_{\text{HII}}$  are almost constant inside the galactic disks. Therefore the dust evacuation occurs in the entire galactic disks once the condition for the dust evacuation is satisfied at the center of disks.

We expect that the dust-to-gas mass ratio is reduced remarkably or even becomes zero due to the dust evacuation. On the other hand, the dust depletion factor  $f_{\text{dep}}$  is  $\sim 0.5$  in the solar neighborhood (Pollack et al. 1994), and it is theoretically suggested to be smaller in very low-metallicity environments (Asano et al. 2013; Rémy-Ruyer et al. 2014). Thus even though the dust is totally evacuated, the left-over gas metallicity is not significantly lower than the original (gas and dust) metallicity.

In the dust evacuated gas, fragmentation would be suppressed because the dust cooling and  $\text{H}_2$  formation on grain surfaces are quenched. Therefore, more massive stars tend to form in such regions.

It is theoretically expected that star-forming clumps can fragment to dense cores of sub-solar mass when the metallicity is higher than the critical value  $Z_{\text{crit}} = 10^{-6} - 10^{-5} Z_{\odot}$  (Omukai et al. 2005; Schneider et al. 2012). However, the observed metallicity distribution of metal-poor stars is better reproduced with the critical metallicity at  $Z_{\text{crit}} = 10^{-4} Z_{\odot}$

(Salvadori et al. 2007), much higher than the theoretical expectation. Reduction of depletion factor  $f_{\text{dep}}$  in low-metallicity environments may explain this difference in the theoretical and empirical critical metallicities  $Z_{\text{crit}}$ . This may be caused by slow dust growth in low-metallicity environments (Asano et al. 2013; Rémy-Ruyer et al. 2014). We expect that the dust evacuation also contributed to reduce the depletion factor. At the metallicity  $Z \sim Z_{\text{crit}}$ , the dust-to-gas ratio  $\mathcal{D}$  is easily reduced by the dust evacuation below the critical value  $\mathcal{D}_{\text{crit}}$ . In order for  $\mathcal{D}$  to exceed  $\mathcal{D}_{\text{crit}}$ , the metallicity needs to be higher than the theoretical critical metallicity in the dust-evacuated gas. Therefore, the dust evacuation boosts the critical metallicity  $Z_{\text{crit}}$  compared with the theoretical prediction for  $f_{\text{dep}}$  similar to the Galactic value.

As the dust size decreases, the radiation force on dust grains becomes weaker due to the lower absorption efficiency. Therefore, small dust grains with the size less than  $\sim 0.01\mu\text{m}$  remain within star-forming clouds despite the stellar radiation feedback. Nozawa et al. (2007) and Schneider et al. (2012) indicated that the small grains of  $\lesssim 0.01\mu\text{m}$  could be destructed in the reverse shock in SN remnants.

Cosmic rays (CRs) and Magnetic fields can suppress the dust evacuation. CRs raise the ionization degree higher than  $\sim 10^{-5}$ , if the source galaxy with  $\text{SFR} \gtrsim 1 M_{\odot}\text{yr}^{-1}$  is within 40 kpc or SN remnants are inside the same galaxy. In this case, the dust evacuation is significantly suppressed due to the Coulomb drag. Also, the magnetic fields can be stronger than  $0.1 \mu\text{G}$  via turbulent small-scale dynamo amplification (Schober et al. 2012), and suppress the dust drift in the vertical direction.

A large fraction of observed metal-poor stars are CEMP stars (Frebel & Norris 2015; Aoki et al. 2006, 2013; Yoon et al. 2016). For formation of CEMP stars, such scenarios as accretion of gases with metals but devoid of dust onto metal-poor stars from interstellar medium (Johnson 2015), mass transfer from the companion star in the binary system (Komiya et al. 2007) or metal enrichment from the faint SNe of the primordial stars (Nomoto et al. 2013) are proposed. The dust evacuation can also explain the observed CEMP star composition by altering the chemical composition of the gas from the original value. The degree of depletion into grains sensitively depends on the metal species: for example, iron is more depleted into grains than carbon, according to the observations of interstellar medium (e.g., Jenkins 2009; Johnson 2015). Therefore, the dust evacuation can enhance the carbon abundance relative to iron.

## ACKNOWLEDGEMENTS

The authors wish to express our cordial thanks to Profs Takahiro Tanaka and Takashi Hosokawa for their continual interest and advices. We also thank Daisuke Nakauchi, Kazu Sugimura and Ryoki Matsukoba for fruitful discussions. We would like to thank to an anonymous reviewer for the constructive comments and advices, especially for Sec. 4. This work is supported in part by MEXT/JSPS KAKENHI grants (KO:25287040, 17H01102, HY:17H04827).

## REFERENCES

Aoki W., et al., 2006, ApJ, 639, 897

- Aoki W., et al., 2013, ApJ, 145, 13  
 Asano R. S., Takeuchi T. T., Hirashita H., Nozawa T., 2013, MNRAS, 432, 637  
 Akimkin V. V., Kirsanova M. S., Pavlyuchenkov Ya. N., Wiebe D. S., 2015, MNRAS, 449, 440  
 Akimkin V. V., Kirsanova M. S., Pavlyuchenkov Ya. N., Wiebe D. S., 2017, MNRAS, 469, 630  
 Barkana R., Loeb A., 2001, Phys. Rep., 349, 125  
 Bianchi S., Schneider R., 2007, MNRAS, 378, 973  
 Blümer J., Engel R., Hörandel J. R., 2009, Prog. Part. Nucl. Phys., 63, 293  
 Bromm V., Ferrara A., Coppi P. S., Larson R. B., 2001, MNRAS, 328, 969  
 Bromm V., Loeb, A. 2003, Nature, 425, 812  
 Chabrier G., 2003, ApJ, 586, 133,  
 Chiao R. Y., Wickramasinghe N. C., 1972, MNRAS, 159, 361  
 Chen Y., Bressan A., Girardi L., Marigo P., Kong X., Lanza A., 2015, MNRAS, 452, 1068  
 Clark P. C., Glover S. C. O., Klessen R. S., Bromm V., 2011, ApJ, 727, 110  
 Crutcher R. M., 1999, ApJ, 520, 706  
 Draine B. T., 2003, ApJ, 598, 1026  
 Draine B. T., 2011a, ApJ, 732, 100  
 Draine B. T., 2011b, Physics of the Interstellar and Intergalactic Medium. Princeton University Press: Princeton, NJ  
 Draine B. T., Lee H. M., 1984, ApJ, 285, 89  
 Draine B. T., Salpeter E. E., 1979, ApJ, 231, 77  
 Draine B. T., Sutin B., 1987, ApJ, 320, 803  
 Dwek E., Galliano F., Jones A. P., ApJ, 662, 927  
 Eisenstein D. J., Hu W., 1998, ApJ, 496, 605  
 Eisenstein D. J., Hu W., 1999, ApJ, 511, 5  
 Ferrara A., Ferrini F., Barsella B., Franco J., 1991, ApJ, 381, 137  
 Frebel A., Norris J. E., 2015, ARA&A, 53, 631  
 Fukushima H., Omukai K., Hosokawa T., 2018, MNRAS, 473, 4754  
 Glover S. C. O., Brand P. W. J. L., 2003, MNRAS, 340, 210  
 Jenkins E. B., 2009, ApJ, 700, 1299  
 Johnson J. L., 2015, MNRAS, 453, 2771  
 Hirano S., Hosokawa T., Yoshida N., Umeda H., Omukai K., Chiaki G., Yorke H. W., 2014, ApJ, 781, 60  
 Hirano S., Hosokawa T., Yoshida N., Omukai K., Yorke H. W., 2015, MNRAS, 448, 568  
 Hosokawa T., Omukai K., Yoshida N., Yorke H. W., 2011, Science, 334,1250  
 Hosokawa T., Hirano S., Kuiper R., Yorke H. W., Omukai K., Yoshida N., 2016, ApJ, 824, 119  
 Hummer D. G., Storey P. J., 1987, MNRAS, 224, 801  
 Inayoshi K., Omukai K., 2011, MNRAS, 416, 2748  
 Ishiki S., Okamoto T., Inoue A. K., 2018, MNRAS, 474, 1935  
 Katz N., 1992, ApJ, 391, 502  
 Koh D., Wise J. H., 2016, MNRAS, 462, 81  
 Komiya Y., Suda T., Minaguchi H., Shigeyama T., Aoki W., Fujimoto M. Y., 2007, ApJ, 658, 367  
 Kroupa P., 2001, MNRAS, 322, 231  
 Larson R. B., 1998, MNRAS, 301, 569  
 Machida M. N., Omukai K., Matsumoto T., Inutsuka S., 2008, ApJ, 677, 813  
 Mathis J. S., Rumpl W., Nordsieck K. H., 1977, ApJ, 217, 425  
 McKee C. F., 1989, ApJ, 345, 782  
 McKee C. F., Ostriker J. P., 1977, ApJ, 218, 148  
 Mo H. J., Mao S., White S. D. M., 1998, MNRAS, 295, 319  
 Morgan H. L., Edmunds M. G., 2003, MNRAS, 343, 427  
 Nomoto K., Kobayashi C., Tominaga N., 2013, ARA&A, 51, 457  
 Nozawa T., Kozasa T., Habe A., Dwek E., Umeda H., Tominaga N., Maeda K., Nomoto K., 2007, ApJ, 666, 955  
 Omukai K., 2000, ApJ, 534, 809  
 Omukai K., Tsuribe T., Schneider R., Ferrara A., 2005, ApJ, 626, 627

- Oh S. P., Haiman Z., 2002, ApJ, 569, 558  
 Osterbrock D. E., Ferland G. J. 2006, in *Astrophysics of Gaseous Nebulae and Active Galactic Nuclei*, ed. D. E. Osterbrock, & G. J. Ferland (2nd ed.; Sansolito, CA: Univ. Sci. Books)  
 Planck Collaboration XIII., A&A, 2016, 594, 13  
 Plume R., Jaffe D. T., Evans N. J. II., Martín-Pintado J., Gómez-González J., 1997, ApJ, 476, 730  
 Pollack J. B., Hollenbach D., Beckwith S., Simonelli D. P., Roush T., Fong W., 1994, ApJ, 421, 615  
 Rémy-Ruyer A., Madden S. C., Galliano F., et al., 2014, A&A, 563, 31  
 Salvadori S., Schneider R., Ferrara A., 2007, MNRAS, 381, 647  
 Santoro F., Shull J. M., 2006, ApJ, 643, 26  
 Schaerer D., 2002, A&A, 382, 28  
 Schneider R., Ferrara A., Natarajan P., Omukai K., 2002, ApJ, 571, 30  
 Schneider R., Ferrara A., Salvaterra R., Omukai K., Bromm V., 2003, Nature, 422, 869  
 Schneider R., Omukai K., Bianchi S., Valiante R., 2012, MNRAS, 419, 1566  
 Schober J., Schleicher D., Federrath C., Glover S., Klessen R. S., Banerjee R., 2012, ApJ, 754, 99  
 Solomon P. M., Rivolo A. R., Barrett J., Yahil A., 1987, ApJ, 319, 730  
 Spitzer L., 1978, *Physical Processes in the Interstellar Medium*. Wiley, New York  
 Stacy A., Bromm V., 2007, MNRAS, 382, 229  
 Stacy A., Bromm V., Lee A. T., 2016, MNRAS, 462, 1307  
 Susa H., Hasegawa K., Tominaga N., 2014, ApJ, 792, 32  
 Todini P., Ferrara A., 2001, MNRAS, 325, 726  
 Wolfire M. G., Hollenbach D., McKee C. F., Tielens A. G. G. M., Bakes E. L. O., 1995, ApJ, 443, 152  
 Weingartner J. C., Draine B. T., 2001, ApJS, 134, 263  
 Yoon J., Beers T. C., Placco V. M., Rasmussen K. C., Carollo D., He S., Hansen T. T., Roederer I. U., Zeanah J., 2016, ApJ, 833, 20

## APPENDIX A: EFFECTS OF COULOMB DRAG

In this paper, we only take the collisional drag force ( $F_{\text{collision}}$ ) into account in calculating the terminal velocity of dust grains. However, as the ionization fraction increases, the acceleration of dust grains will be regulated by the Coulomb drag force ( $F_{\text{Coulomb}}$ ). Here we investigate the effect of the Coulomb drag on the terminal velocity of dust grains. The total drag force is given by (Draine & Salpeter 1979):

$$\begin{aligned} F_{\text{drag}} &= F_{\text{collision}} + F_{\text{Coulomb}} \\ &= 2\pi a^2 k T n_{\text{H}} \left[ G_0(s) + x_e \phi^2 \ln(\Lambda) G_2(s) \right], \quad (\text{A1}) \end{aligned}$$

where

$$G_0 = \frac{8s}{3\sqrt{\pi}} \left( 1 + \frac{9\pi}{64} s^2 \right)^{1/2}, \quad (\text{A2})$$

$$G_2 = \frac{s}{(3\sqrt{\pi}/4 + s^3)}, \quad (\text{A3})$$

$$\phi = eU/kT, \quad (\text{A4})$$

$$s = (mv_d^2/2kT)^{1/2}, \quad (\text{A5})$$

$$\Lambda = \frac{3}{2ae|\phi|} \left( \frac{kT}{\pi x_e n_{\text{H}}} \right)^{1/2}, \quad (\text{A6})$$

$x_e$  is the ionization fraction and  $U = z_{\text{grain}}e/a$  is Coulomb potential of dust grains. The Coulomb potential is  $U =$

$z_{\text{grain}}e/a$ , where  $z_{\text{grain}}$  is the dust charge. Here we set the gas temperature at  $T = 100$  K. Below, we evaluate the terminal velocities of grains for different values of ionization fraction.

The Coulomb drag sensitively depends on the grain charge, which is determined by the balance between the following three processes; (1) ion collisions  $J_{\text{ion}}$ , (2) electron collisions  $J_e$ , (3) photoelectric effect  $J_{\text{pe}}$ :

$$J_{\text{pe}}(z_{\text{grain}}) + J_{\text{ion}}(z_{\text{grain}}) = J_e(z_{\text{grain}}). \quad (\text{A7})$$

The rate of collisional effect is given as (Weingartner & Draine 2001)

$$J_i = n_i f_i \sqrt{\frac{8kT}{\pi m_i}} \pi a^2 \bar{J}(a, T, z_{\text{grain}}), \quad (\text{A8})$$

where  $f_i$  is the probability that gas particles deliver charge to dust grains when they collide. We use  $f_i = 0.5$  for electrons and 1 for ions (Akimkin et al. 2015). Expression for  $\bar{J}$  in Equation (A8) is given by (Draine & Sutin 1987):

$$\bar{J}(\tau, \nu) = \begin{cases} 1 + \left(\frac{\pi}{2\tau}\right)^{1/2} & (\nu = 0) \\ \left[1 - \frac{\nu}{\tau}\right] \left[1 + \left(\frac{2}{\tau-2\nu}\right)^{1/2}\right] & (\nu < 0) \\ \left[1 + (4\tau + 3\nu)^{-1/2}\right]^2 \exp(-\theta_\nu/\tau) & (\nu > 0) \end{cases} \quad (\text{A9})$$

where  $\tau$ ,  $\nu$  and  $\theta_\nu$  are

$$\tau = \frac{akT}{q_i^2}, \quad (\text{A10})$$

$$\nu = \frac{Ze}{q_i}, \quad (\text{A11})$$

and

$$\theta_\nu = \frac{\nu}{1 + \nu^{-1/2}}. \quad (\text{A12})$$

In Equation (A10) and (A11),  $q_i$  represents the charge of dust grains, and we use  $q_i = 1$  here. Also, the photoelectric rate is given by

$$J_{\text{pe}} = \pi a^2 \int d\nu \left( \frac{c u_\nu}{h\nu} \right) Y_{\text{pe}}(\nu, a, Z) Q_{\text{abs}}(\nu), \quad (\text{A13})$$

where  $Y_{\text{pe}}$  is photoelectric yield (Weingartner & Draine 2001),  $u_\nu$  is monochromatic radiation energy density. As in Figure 3, the efficiency factor  $Q_{\text{abs}}$  for absorption is calculated by Mie theory using the dielectric function given by Draine & Lee (1984) and Draine (2003).

We estimate  $u_\nu$  by summing up the contributions from stars according to the IMF (Eq. 8). Figure A1 shows the specific luminosity in the case with the SFE  $\epsilon_* = 0.1$ . With the specific luminosity, the radiation energy density is given as  $u_\nu = L_\nu/(4\pi r^2 c)$ . Thus,

$$J_{\text{pe}} = \frac{\pi a^2 L_*}{4\pi r^2} \left\langle \frac{Y_{\text{pe}} Q_{\text{abs}}}{h\nu} \right\rangle, \quad (\text{A14})$$

where  $L_*$  is the bolometric luminosity. The bracket represents the mean value in the frequency range  $\nu_{\text{min}} - \nu_{\text{max}}$ :

$$\left\langle \frac{Y_{\text{pe}} Q_{\text{abs}}}{h\nu} \right\rangle = \frac{\int_{\nu_{\text{min}}}^{\nu_{\text{max}}} d\nu \left( \frac{L_\nu}{h\nu} \right) Y_{\text{pe}}(\nu, a, Z) Q_{\text{abs}}(\nu)}{\int_{\nu_{\text{min}}}^{\nu_{\text{max}}} d\nu L_\nu}. \quad (\text{A15})$$

Here we take the Lyman-limit frequency as  $\nu_{\text{max}}$ , assuming

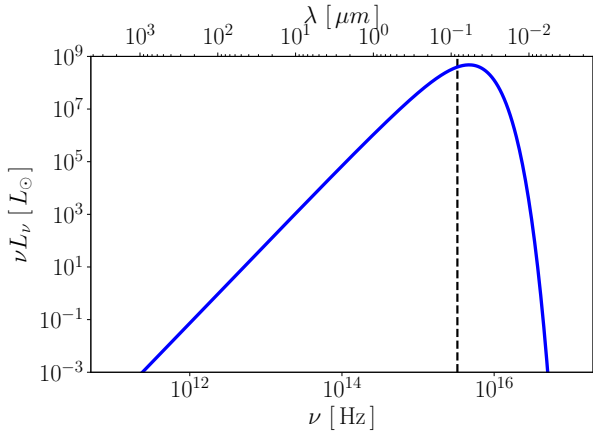


**Figure A1.** Spectral energy distribution of a star cluster formed in a star-forming cloud with mass  $M_{\text{cl}} = 10^6 M_{\odot}$ , radius  $R_{\text{cl}} = 10$  pc, and SFE  $\epsilon_* = 0.1$ . We set  $m_{\text{ch}} = 10 M_{\odot}$  for Larson IMF. The vertical dashed line represents Lyman limit  $0.0912 \mu\text{m}$ .

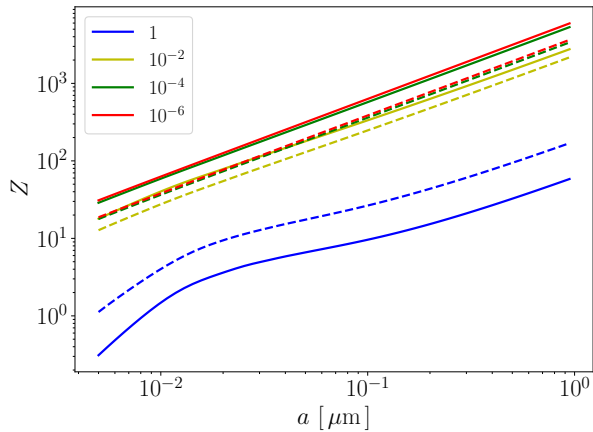


**Figure A2.** Grain charge as a function of grain radius. The different lines correspond to the different ionization fractions,  $x_e = 1$  (blue),  $10^{-2}$  (green),  $10^{-4}$  (yellow), and  $10^{-6}$  (red).

that Lyman-continuum photons cannot escape from the HII regions.

In the following, we consider the cases of star-forming clouds with mass  $M_{\text{cl}} = 10^6 M_{\odot}$  and radius  $R_{\text{cl}} = 10$  pc, and set  $\epsilon_* = 0.1$  and characteristic stellar mass  $m_{\text{ch}} = 10 M_{\odot}$  for the Larson IMF. Dust grain charges are computed for four different ionization fractions  $x_e = 1, 10^{-2}, 10^{-4}$ , and  $10^{-6}$ . Figure A2 shows the grain charge as a function of its size. The grain charge decreases as the ionization fraction increases. This is because free electrons are adsorbed to grains efficiently for the higher ionization fraction, thereby offsetting their photoelectrically induced positive charge. Yet, the energy of photons must exceed the Coulomb potential for grains to eject electrons. The photoelectric process thus becomes inefficient for the Coulomb potential exceeding  $\sim 13.6$  eV. Even at  $x_e \sim 10^{-4}$ , the Coulomb potential

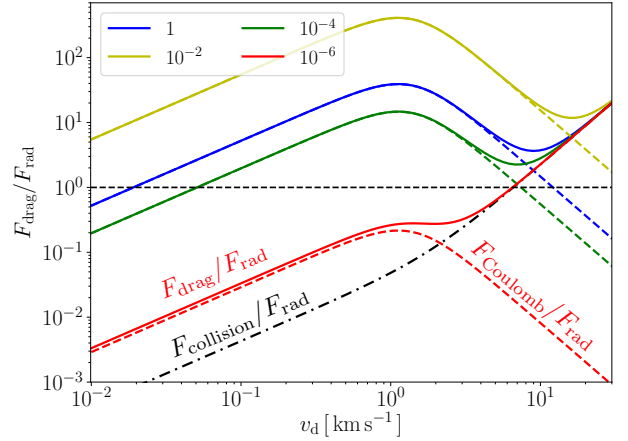


**Figure A3.** The ratio of the drag force to the radiation force on to a graphite grain of  $0.1 \mu\text{m}$ . The different lines correspond to the different ionization fraction,  $x_e = 1$  (blue),  $10^{-2}$  (green),  $10^{-4}$  (yellow), and  $10^{-6}$  (red). The contribution by the Coulomb drag  $F_{\text{Coulomb}}$  and the collisional drag force  $F_{\text{collision}}$  are shown by dashed and dot-dashed lines, respectively. The horizontal dashed line represents the drag force being equal to the radiation force.

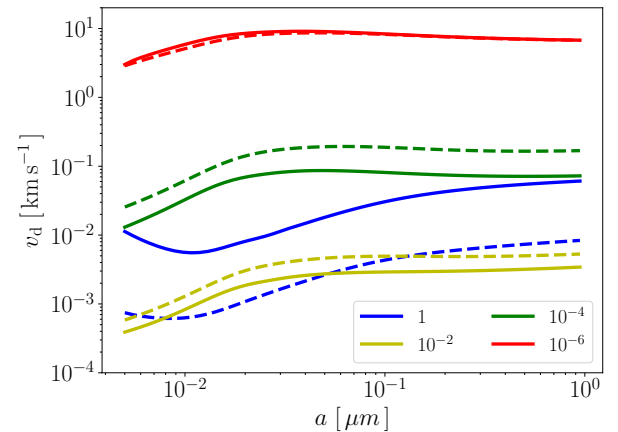


**Figure A4.** Terminal velocity of grains as a function of their size. The solid and dashed lines represent graphite and silicate grains, respectively. The different lines correspond to the different ionization fractions,  $x_e = 1$  (blue),  $10^{-2}$  (green),  $10^{-4}$  (yellow), and  $10^{-6}$  (red).

becomes close to the Lyman limit. Thus, the grain charge does not increase remarkably at  $x_e \lesssim 10^{-4}$ .

Figure A3 shows the ratio of the drag force to the radiation force on to a graphite grain of  $0.1 \mu\text{m}$  as a function of the grain velocity. With the ionization fraction higher than  $10^{-4}$ , the Coulomb drag becomes equal to the radiation force at  $v_d < 10^{-1} \text{ km s}^{-1}$ , and the grains cannot move fast enough to decouple from the gas component. On the other hand, in the case of  $x_e = 10^{-6}$ , the Coulomb drag is minor and the collisional drag instead balances with the radiation force. In this case, we can calculate the terminal velocity of grains, ignoring the Coulomb drag force, as in Section 2.2. Figure

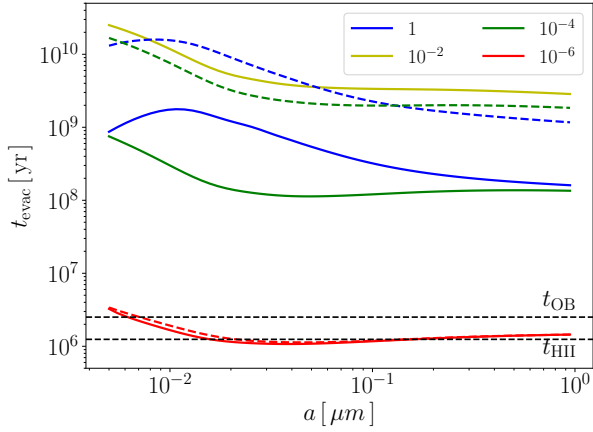


**Figure A5.** Dust evacuation time  $t_{\text{evac}}$  as a function of the grain size in the case with  $(M_{\text{cl}}, R_{\text{cl}}, \epsilon_*) = (10^6 M_{\odot}, 10 \text{ pc}, 0.1)$ . As in Figure A4, colors correspond to different ionized fractions. Also shown are the expansion time of HII regions  $t_{\text{HII}}$  and lifetime of OB stars  $t_{\text{OB}}$ .

A4 shows the terminal velocity of grains, set by the balance  $F_{\text{rad}} = F_{\text{collision}} + F_{\text{Coulomb}}$ , as a function of the size. As expected, the terminal velocity is significantly reduced due to the Coulomb drag when  $x_e > 10^{-6}$ . At  $a \lesssim 0.1 \mu\text{m}$ , the terminal velocity decreases for smaller dust size, because of the lower radiation absorption efficiency (Fig. 3). Figure A5 shows the dust evacuation time  $t_{\text{evac}}$  calculated by Equation (17). At  $x_e = 10^{-6}$ , grains in the size range  $2 \times 10^{-2} - 10^{-1} \mu\text{m}$  satisfy the condition of dust evacuation, while these of  $a < 2 \times 10^{-2} \mu\text{m}$  ( or  $a > 10^{-1} \mu\text{m}$  ) does not. Therefore, small grains may remain in the star-forming region if the size distribution extends over a wide range.

This paper has been typeset from a  $\text{\TeX}/\text{\LaTeX}$  file prepared by the author.